# Stony Brook University

# Modeling brain structures from hundreds of hypoglossal motoneurons to millions of cerebellar cells

A Dissertation Presented

by

**Heraldo Memelli**

to

The Graduate School

in Partial Fulfillment of the

Requirements

for the Degree of

**Doctor of Philosophy**

in

**Computer Science**

Stony Brook University

**December 2014**

**Stony Brook University**

The Graduate School

**Heraldo Memelli**

We, the dissertation committee for the above candidate for the

Doctor of Philosophy degree, hereby recommend

acceptance of this dissertation.

**Larry D. Wittie – Dissertation Advisor**
Professor, Department of Computer Science

**Scott A. Smolka – Chairperson of Defense**
Professor, Department of Computer Science

**Irene C. Solomon**
Professor, Department of Physiology and Biophysics

**Bardia Behabadi – External Member**
Senior Research Scientist, Qualcomm Research

This dissertation is accepted by the Graduate School

Charles Taber
Dean of the Graduate School

Abstract of the Dissertation

**Modeling brain structures**
**from hundreds of hypoglossal motoneurons to millions of cerebellar cells**

by

**Heraldo Memelli**

**Doctor of Philosophy**

in

**Computer Science**

Stony Brook University

**2014**

Computational neuroscience is a rapidly growing field in the quest to discover how the human brain works. Mathematical modeling and computer simulations increasingly help neuroscientists test hypotheses and explore neuronal mechanisms from the level of single cells to billions of neurons. In this PhD Dissertation, we have implemented and analyzed computational models of two mammalian brain structures: the hypoglossal nucleus and the cerebellum.

As a first project, we have developed a detailed computational model for a network of Hypoglossal Motoneurons (HMs). HMs are located in the brainstem and exhibit synchronous firing activity. They are coupled by gap junctions, direct electrical links between neighboring neurons. We have simulated HM networks with hundreds of neurons for a quantitative analysis of changes in their synchronized behavior under different conditions. Some of the conditions and mechanisms analyzed include: simulated gap junction uncoupling, changes in premotor excitatory

input current strength, modulation of HM firing frequency, and the emergence of different firing groups.

A major ongoing project in our lab is the building of a unified efficient system for creation, simulation, and visualization of large-scale models of brain structures. These models are morphologically representative neuronal networks which include neurons and synapses of different types. We have used this system to create models of the cerebellum, the "little brain" that coordinates complex motor activities. The cerebellum large-scale models consist of millions of neurons and billions of synapses. We have run numerous simulations on PCs and on Blue Gene supercomputers to analyze firing activity in the cerebellar circuits.

The approaches for the two projects are somewhat different. The first project focuses on the biophysical details of the model and the resulting biological interpretations of specific cellular mechanisms. The second project emphasizes performance and simulations of very large networks of different cell types. Both projects provide useful insight into various mechanisms in the respective simulated networks.

*Dedicated to my parents, Agim and Violeta Memelli.*

# Contents

# List of Tables

# List of Figures

# Preface

Work for the first project, presented in Chapter 2, was done mostly as a collaboration with the Solomon lab in particular with Prof. Irene Solomon and Dr. Kyle Horn from the Department of Physiology and Biophysics. Work for the second project was done mainly in the Wittie lab in the Department of Computer Science in collaboration with Jack Zito and Remy Oukaour, under the supervision of Prof. Larry Wittie. There was constant collaboration between the two labs.

**List of Peer-Reviewed Journal Publications**

- *Using a computational model to analyze the effects of firing frequency on synchrony of a network of gap junction-coupled hypoglossal motoneurons*
  H. Memelli, K. G. Horn, L. D. Wittie and I. C. Solomon.
  In Progress in Brain Research: Breathing, Emotion and Evolution, 2014.

- *Analyzing the effects of gap-junction blockade on neural synchrony via a motoneuron network computational model*
  H. Memelli, K. G. Horn, L. D. Wittie and I. C. Solomon.
  In Computational Intelligence and Neuroscience, 2012.

- *Emergent central pattern generator behavior in gap junction coupled Hodgkin-Huxley style neuron model*

K. G. Horn, H. Memelli and I. C. Solomon.

In Computational Intelligence and Neuroscience, 2012.

- *Application of a Staggered-Walk algorithm for generating large-scale morphological neuronal networks*

  J. Zito, H. Memelli, K. G. Horn, L. D. Wittie and I. C. Solomon.

  In Computational Intelligence and Neuroscience, 2012.

**From Other Projects**

- *Self-referential forces are sufficient to explain different dendritic morphologies*

  H. Memelli, B. Torben-Nielsen, J. Kozloski.

  Frontiers in Neuroinformatics, 2013.

- *Optimizing restriction site placement for synthetic genomes*

  P. Montes, H. Memelli, C. Ward, J. S. B. Mitchell and S. Skiena.

  In Combinatorial Pattern Matching, 2010 and in Information and Computation, 2012.

**Conference Posters and Presentations**

- *Influence of timing and magnitude of input current on network synchrony in a computational model of gap junction-coupled hypoglossal motoneurons*
  H. Memelli, K. G. Horn, L. D. Wittie and I. C. Solomon. Society for Neuroscience Annual Meeting, San Diego CA, November 2013.

- *Investigating behavior of hypoglossal motoneurons using a computational network model*
  H. Memelli, K. G. Horn, L. D. Wittie and I. C. Solomon. Society for Neuroscience Annual Meeting, New Orleans LA, October 2012.

- *Simulating a network of hypoglossal motoneurons (HMs) with full and reduced mathematical models*
  H. Memelli, K. G. Horn, L. D. Wittie and I. C. Solomon, Oxford Conference, Almelo Netherlands, August 2012.

- *Gap-junction coupling in a computational model of the hypoglossal motor nucleus*
  H. Memelli, K. G. Horn, L. D. Wittie and I. C. Solomon. Experimental Biology, San Diego CA, April 2012.

- *A computational model of the entire hypoglossal motor nucleus*
  H. Memelli, K. G. Horn, L. D. Wittie and I. C. Solomon. Society for Neuroscience Annual Meeting, Washington DC, October 2011.

- *Investigating hypoglossal motor nucleus behavior using a computational network model*
  H. Memelli, K. G. Horn, L. D. Wittie and I. C. Solomon. Experimental Biology, Washington DC, April 2011.

- *Efficient simulation and visualization of millions of cerebellar neurons*
  J. Zito, H. Memelli, R. Oukaour, I. C. Solomon and L. D. Wittie. Society for Neuroscience Annual Meeting, Washington DC, November 2014.

- *Large-scale brain simulations: modeling a cat cerebellum*
  H. Memelli, J. Zito, R. Oukaour, I. C. Solomon and L. D. Wittie. Society for Neuroscience Annual Meeting, San Diego CA, November 2013.

- *Generating large-scale brain tissue models for simulations on supercomputers*
  J. Zito, H. Memelli, I. C. Solomon and L. D. Wittie. Society for Neuroscience Annual Meeting, New Orleans LA, October 2012.

- *Deriving billions of details for fast brain models from brain tissue statistics - INIT*
  L. D. Wittie, H. Memelli, J. Zito and I. C. Solomon. Society for Neuroscience Annual Meeting, Washington DC, November 2011.

- *Billion-neuron memory models in slender blue genes*
  L. D. Wittie, R. Welsch and H. Memelli. Society for Neuroscience Annual Meeting, San Diego CA, November 2010.

# Acknowledgements

I would like to thank my advisor Larry Wittie - for guiding me in the difficult path to the PhD and for teaching me so much more than what can be listed in an "Acknowledgement" sentence; Irene Solomon, my second mentor and co-advisor, for supporting me in countless ways in my journey into an interdisciplinary field; Scott Smolka - for his time as the chair of my committee throughout all the milestones of my PhD and for his always helpful feedback; Jack Zito - for spending countless Thursday nights and Sunday afternoons with me in lab and for providing his invaluable real-world technical expertise; Kyle Horn - for being the ideal collaborator and co-author; Remy Oukaour - for literally helping us see the results of our work; Bardia Behabadi - for being a great mentor outside of Stony Brook and for his time as part of my committee; James Kozloski - for being a great mentor, collaborator and friend outside of Stony Brook.

I would like to thank many other amazing people in Stony Brook University's department of Computer Science: Prof. IV Ramakrishnan - for always being supportive; Prof. Steve Skiena - for introducing me to the world of algorithms and for guiding me to my first academic publication; the administrative staff, in particular Cindy Scalzo - for being the most helpful and patient person in the world.

At a personal level, I would like to thank the many wonderful friends that I made in this 6-year journey and that will always be a part of my life; in particular Pablo Montes for all the coffee breaks and for always being a reliable support since

the first day. I would also like to thank my old friends Kliti Kodra and Edi Naco and their families for making me feel at home away from home especially in my first years in the US. In addition, I would like to thank my aunt Lindita Adili for guiding me in the very first steps of my education and help me build the strong foundations that were crucial in my success. Last, but not least, I would like to express immense gratitude to my parents, Agim and Violeta, to my brother, Gledi, and my girlfriend, Estefania, for their unconditional love and support.

# Chapter 1

# Introduction

## 1.1 Neuroscience and Computational Modeling

It is widely accepted that understanding the brain is one of the most challenging intellectual tasks of the 21st century, "the century of the brain". The human brain contains over one hundred billion nerve cells or neurons and roughly one quadrillion ($10^{15}$) connections, or synapses, between neurons. How this complex "machine" functions is still a vast mystery.

The neuron is the basic building block of the brain and the nervous system. It is an electrically excitable cell that is specialized in inter-cellular communication. The main function of a neuron is to receive input "information" from thousands of other neurons through its numerous dendrites, to process that information, and then to send "information" as output to other neurons through its axon.

Synapses are the main type of connections between neurons (usually axon-to-dendrite) through which "information" flows from one neuron to another by electro-chemical signals. The neuron that is sending the signal through its axon is called the pre-synaptic neuron, and the receiving neuron is defined as post-synaptic. There are dozens of types of neurons in mammalian nervous systems and they vary in shape, size, and electrical behavior but they share many common characteristics

that distinguish them from other cells in the body.

The signals produced by the neurons are called *action potentials*. An action potential is an all-or-nothing positive spike in the membrane voltage. As the result of the input from other cells, the membrane voltage can become more positive than the negative resting potential ("depolarized"). If the potential becomes depolarized enough to cross a threshold, the neuron generates an action potential, or in other words, it fires a spike. For a more comprehensive review of neuroscience please see [51].

Computational neuroscience is a relatively new field that has been rapidly growing in the last decade and is going to be crucial in the quest to discover how the human brain works. Theoretical models give scientist the tools and capabilities to test hypotheses that are impossible or impractical to test in vivo.

Mathematical models of varying complexity have been developed for neurons. Those models range from the detailed but computationally expensive Hodgkin-Huxley (HH) neuron model [30], to simpler Integrate-and-Fire (IF) models, like the Izhikevich model [34].

Several research groups, rather than focusing on precise details in individual neurons, seek to build networks that consist of millions or even billions of neurons to reach scales where mass neuronal effects emerge. The different levels of biological accuracy or complexity are determined by the kind of questions that these models are targeting.

## 1.2 Modeling Single Neurons

### 1.2.1 Hodgkin-Huxley Models of Neurons

Biologically plausible models of neuronal cells are inspired by considering each cell as an electrical circuit. Since the bi-layer membrane encasing each neuron is impermeable to ions, it acts as an electrical capacitor that accumulates electric charges by blocking their diffusion. In addition, specific ion channels embedded in the membrane are selectively permeable to certain ions under some conditions, letting part of the membrane act as a variable resistor.

In 1952, Hodgkin and Huxley developed a model that, even today, is considered useful and reasonably accurate. The model approximates the main ionic mechanisms behind the generation of action potential "firing spikes" in the giant axon of a squid [30]. It takes the form of a set of ordinary differential equations (ODEs) that contain one voltage-based differential equation, and several other differential equations for each gating variable. The passive properties of such models can be readily derived from Kirchoff's laws.

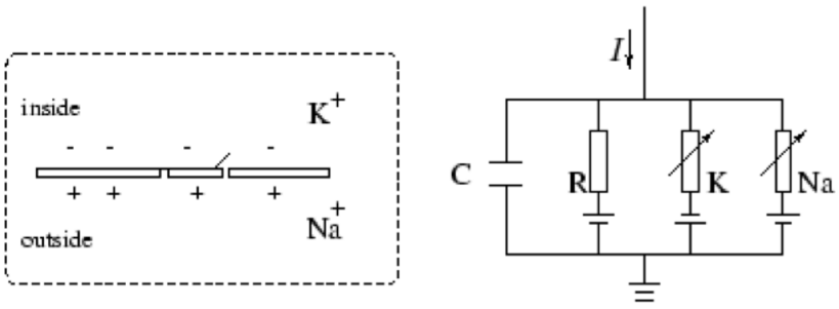


Figure 1: Hodgkin-Huxley diagram

The HH model consists of four nonlinear ordinary differential equations, as

shown in Equation 1 that keep track of the major currents that can be observed in the squid neuron: the capacitive membrane current (C), the sum of external input currents from other neurons (I), a potassium $K^+$ ion current, a sodium Na+ ion current, and a general "Leak" current (represented by the generic resistance R in the diagram) that collectively accounts for the movement of other ions, mainly chloride $Cl^-$.

The model keeps track of conductances, the g-variables in Equation 1 for each ion and it has non-linear gating variables for the $K^+$ and $Na^+$ ion channels (the m, n, h variables). The likelihood of any given gate *x* being open is governed by its steady state variable value (Equation 2). Since gates do not open and close instantaneously, the time constants equations are introduced (Equation 3).

$$C\frac{dV}{dt} = I_{input} + g_{Na}(E_{Na} - V) + g_K(E_K - V) + g_L(E_L - V) \tag{1}$$

$$g_{Na} = \bar{g}_{Na}m^3h \quad g_K = \bar{g}_K n^4 \quad g_L = \bar{g}_L \tag{2}$$

$$\frac{dx}{dt} = \frac{x_\infty(V) - x}{\tau_x(V)} \; where \;\; x = m, n, h \tag{3}$$

The HH model is considered biologically plausible by neuroscientists. The main reason is that experimentalists can adjust model parameters that control ion flow at the cellular level to match the observed electrical activity of many specific types of neurons.

The fact that the HH model has so many nonlinear differential equations (dV, dm, dn and dh) makes it quite computationally expensive. Computational neuroscientists often add even more equations to the standard HH model to account for other mechanisms, such as the movement of calcium ($Ca^{2+}$) ions. These additions make the model more accurate but add to the computer time needed to simulate it.

### 1.2.2 Integrate and Fire Models

Because of the computational complexity of the HH model, many modelers of neuronal networks have focused their attention on computationally simpler classes of neuron models. Leaky IF is the simplest of the standard models used in modeling large networks of neurons [10].

$$\begin{gathered} \frac{dx}{dt} = -\frac{x}{\tau} + x_{input} \\ if(x \geq x_{threshold})\{ \\ x = x_{reset} \\ \} \end{gathered} \tag{4}$$

The single Equation 4 for dx and the threshold test for firing are the heart of all Leaky IF models. The $-x/t$ term causes membrane potential x to decay exponentially over time if the neuron does not receive new synaptic inputs $x_{input}$. Spikes are generated artificially whenever the cell voltage exceeds the "threshold" and then the potential "resets" to a constant pre-defined value.

The model is quite computationally simple because it takes only 4 to 10 (depending on specific implementation) floating-point operations for each time step for each neuron [34]. However, this type of model lacks biological plausibility, not only because it does not take into account the biological details of different ion channels but also because it cannot display many complex spiking behaviors such as tonic bursting or threshold variability [34].

$$\frac{dV}{dt} = 0.04v^2 + 5v + 140 - u + I_{ext} \tag{5}$$

$$\frac{du}{dt} = a(bv - u) \tag{6}$$

$$if(v \geq 30mV)\{$$
$$v = c$$
$$u+ = d$$
$$\}$$

To answer many interesting questions about brain mechanisms, scientists need to simulate large-scale networks of biologically motivated spiking neuron models. The problem is that models in the HH family are very computationally expensive, limiting the sizes and efficiency of simulated networks. The purest IF models are often too simplistic and do not offer a variety of firing patterns. What is needed is a neuron model much more computationally simple than HH but which retains enough biophysical detail to at least produce the variety of firing patterns exhibited by most real neurons.

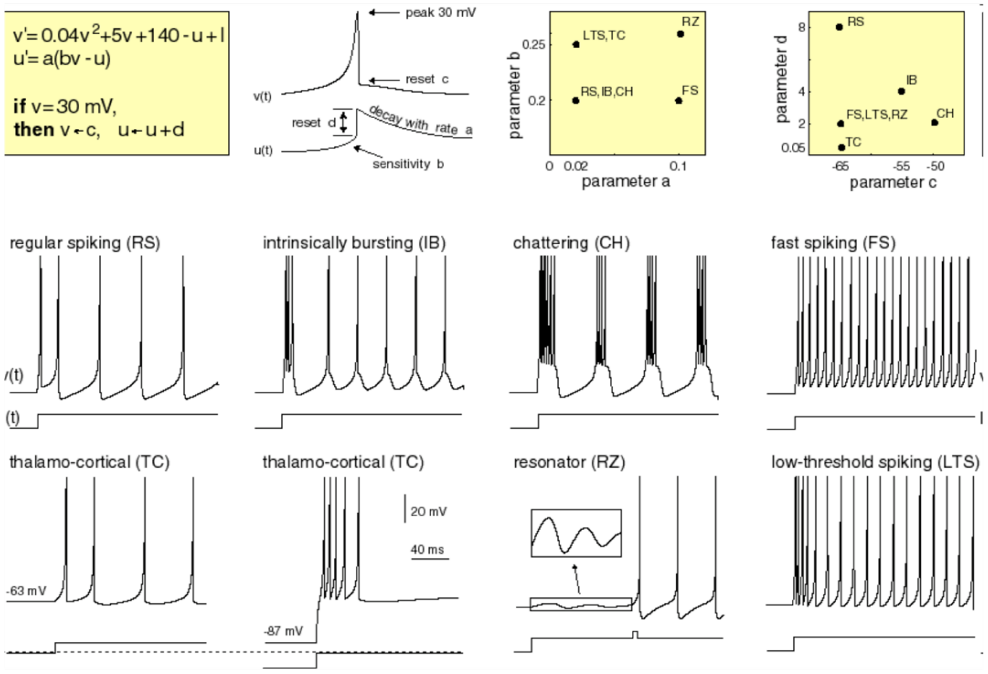


Figure 2: Izhikevich neuron model. (Adapted from [34]).

Eugene Izhikevich has developed a neuron model that is almost as simple as

the standard Integrate-and-Fire but which can model a large variety of the firing patterns seen in neurons in the brain [34]. The two Izhikevich equations, (5) and (6), and the firing threshold and reset condition are shown above. According to Izhikevich, his model is roughly 100 times more computationally efficient than the HH model [34]. Just by changing the values of four parameters (a,b,c,d), the two equations plus the threshold condition and reset can realistically model the firing behavior of many types of neurons observed experimentally, as shown in Figure 2.

## 1.3 Modeling Networks of Neurons

Although modeling single neurons with HH equations can give useful results, the most common modeling work in computational neuroscience involves simulations of networks of neurons. These networks can be very different in terms of size and complexity, sometimes modeling large parts of the brain or even the brain of whole organisms.

Simulating brain structures with large-scale neuronal models is extremely useful because it lets researchers precisely manipulate features of simulated neural tissues and observe both local and global properties of neural systems. During the last decade, large-scale brain modeling has risen in prominence, with a wide range of publications on brain-scale models [2, 23, 33, 37].

Most large-scale modeling research groups focus either on networks that are highly realistic down to the individual axon collaterals and dendrite branches of each neuron [39] or on systems simplified enough to simulate in huge-scale on massively parallel hardware [2, 29, 37].

## 1.4 Our Work

Our work fits somewhere in between the extremes of highly detailed biophysical networks and huge-scale simplified networks.

For our first project, we have developed a computational model of a network of Hypoglossal Motoneurons (HMs), which are located in the brainstem and control the tongue muscles. They are coupled by gap junctions, direct electrical links between neighboring neurons. The mathematical model of HMs captures in great biophysical detail the neurons' ionic currents and firing activity. We have simulated HM networks with hundreds of neurons for a quantitative analysis of their synchronized firing activity. The main goal of this investigation is to shed light on the factors that influence the synchronized behavior of this small network of motoneurons.

BOSS is the main ongoing project of our lab. It is a unified system for creation, simulation, and visualization of large-scale models of brain structures. These models are morphologically representative neuronal networks and include neurons of different types, learning synapses and gap junctions. The first structure that we have focused on is the cerebellum. We have built large-scale models of cerebellar tissue consisting of up to millions of neurons and billions of synapses to match mammalian cerebellar literature. We run many simulations (on PCs and on Blue Gene supercomputers) to test hypotheses related to the functioning of the cerebellum.

# Chapter 2

# Network of Hypoglossal Motoneurons

## 2.1 Biological Background: Hypoglossal Motoneurons and the Hypoglossal Nucleus

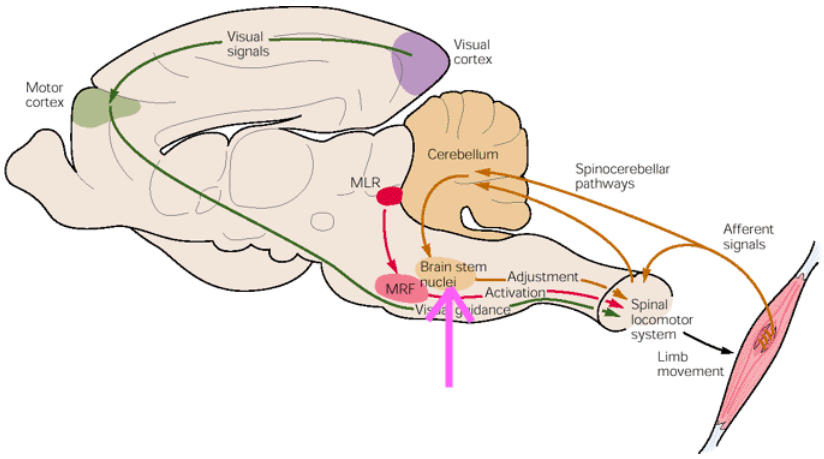


Figure 3: Illustration of rat brain. Adapted from [35].

Hypoglossal motoneurons (HMs) are part of the hypoglossal nucleus which is located in the brainstem and plays an important role in controlling tongue movements. The rat brain, illustrated in Figure 3, shows where the brainstem nuclei are

located (under the cerebellum, in the pathways that lead to the spinal cord). Figure 4 illustrates even more specifically where the HMs are located in the sliced rat brainstem, with the Hypoglossal Nucleus being shown as XII and colored in red.

HMs participate in a variety of upper airway behaviors, including but not limited to swallowing, breathing, suckling, speech, and maintaining upper airway patency [24]. Subsequently, they are of particular interest, as a failure in these neurons can disfacilitate the tongue, rendering an airway obstruction. This could potentially exacerbate hypoxic conditions, and may potentially contribute to sudden infant death syndrome (SIDS) and obstructive sleep apnea.

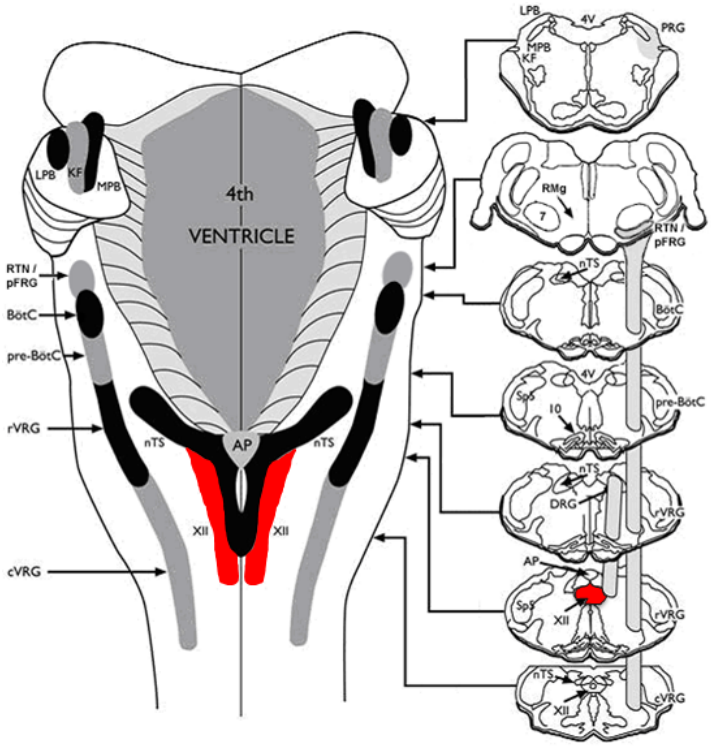


Figure 4: Location of the HMs in the brainstem of the rat. (Adapted from [24].)

## 2.2 The HM Network Model

### 2.2.1 The Hypoglossal Motoneuron Model as an Extended Hodgkin-Huxley Model

The neurons in this project were modeled using ionic current equations from the rat HM mathematical model generated by Purvis and Butera [52]. They developed a single-compartment, electrophysiological, HM model based primarily on experimental data from neonatal rat HMs.

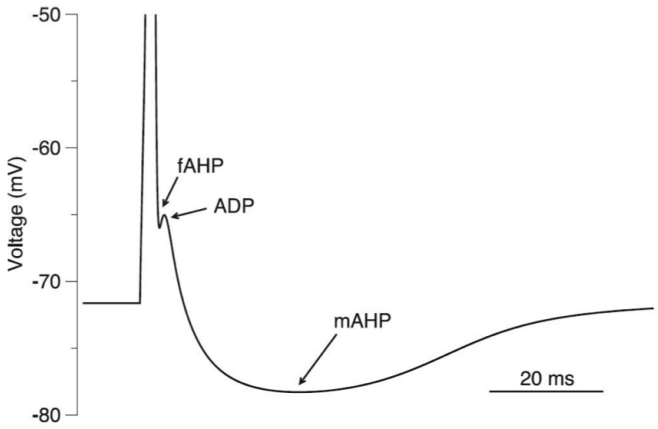


Figure 5: HM spike details

The model is able to reproduce the fine features of the HM action potential: the fast afterhyperpolarization (fAHP), the afterdepolarization (ADP), and the medium-duration afterhyperpolarization (mAHP), as illustrated in Figure 5. The model also reproduces the repetitive firing properties seen in neonatal HMs and replicates the neuron's response to pharmacological experiments. As such, it is suitable to be used for studying the role of specific ionic currents in HM firing.

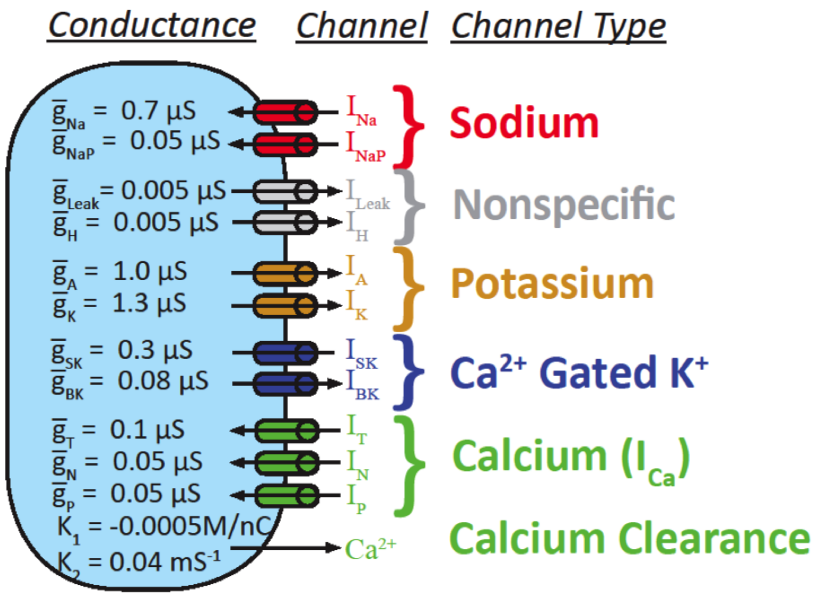


Figure 6: HM model illustration of all channels and parameter values

The HM model belongs to the HH category of models, but it is extended with a few additional ion channels. Equation 7 below presents all the ion currents of the model. More specifically, these myriad ion channels include the voltage-gated category: sodium, potassium, and calcium channels; the ion-activated category: $Ca^{2+}$-activated $K^{+}$ channels, $Ca^{2+}$-activated $Na^{+}$ channels, and $K^{+}$-activated $Na^{+}$ channels; and leak channels. Figure 6 illustrates all the channels that are controlled by Equation (7). The $\bar{g}$ values represent the maximum conductance and they are given as parameter values in [52].

$$
\begin{aligned}
C\frac{dV}{dt} =& I_{input}(t) + \bar{g}_{leak}(E_{leak} - V) + \bar{g}_{Na} m_{Na}^3 h_{Na}(E_{Na} - V) \\
&+ \bar{g}_{Na,p} m_{Na,p} h_{Na,p}(E_{Na} - V) + \bar{g}_K n_K^4 (E_K - V) \\
&+ \bar{g}_A m_A h_A (E_K - V) + \bar{g}_h m_h (E_h - V) \\
&+ \bar{g}_{SK} z_{SK}^2 (E_K - V) + \bar{g}_{BK} b_{BK} (E_K - V) \\
&+ \bar{g}_T m_T h_T (E_{Ca} - V) + \bar{g}_N m_N h_N (E_{Ca} - V) \\
&+ \bar{g}_P m_P (E_{Ca} - V)
\end{aligned} \tag{7}
$$

## 2.3 Gap Junctions

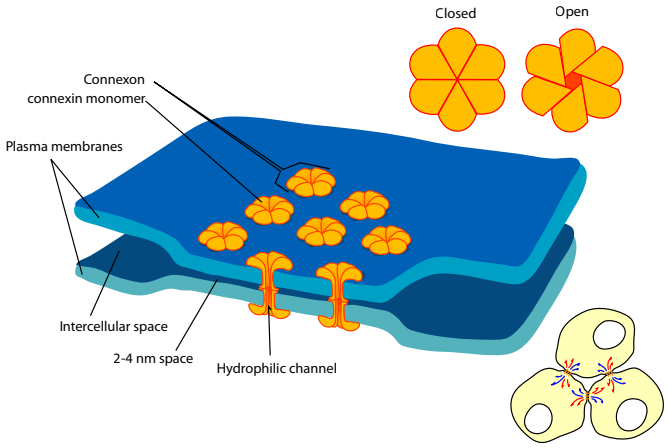


Figure 7: Gap junctions between neurons.(From: Wikimedia Commons)

Gap junctions (also known as electrical synapses) are intercellular channels (illustrated in Figure 7) between neurons and are found in many parts of the mammalian central nervous system (CNS) [7, 14]. They are direct electrical links between adjacent neurons. In the brainstem and spinal cord, gap junction proteins

and/or functional gap junction coupling have been reported in various nuclei including the locus coeruleus, nucleus of the solitary tract (NTS), hypoglossal motor nucleus (HMN), phrenic motor nucleus (PMN), vestibular nucleus, and inferior olivary nucleus [1, 5, 7, 14]. Figure 8, adapted from [16], shows some examples of electrical coupling via gap junctions in different areas of the brain. In the figure, we can clearly see the effect that the presence of the gap junctions has in the membrane potential of a (lower) neuron that is connected to another (upper) neuron that just spiked.

Often gap junctions are present in CNS areas that require synchronized firing activity. They appear to play an important role in a number of vital functions, including respiration, where they influence overall respiratory control and central $CO_2$ chemoreception [14, 19, 61]. To this end, previous reports have identified the gap junction proteins connexin26 (Cx26), connexin32 (Cx32), and connexin36 (Cx36) in neurons within respiratory regions of the rat brainstem [14, 59, 60, 63] and functional blockade of gap junctions has been shown to alter various aspects of respiratory-related activities [9, 60].

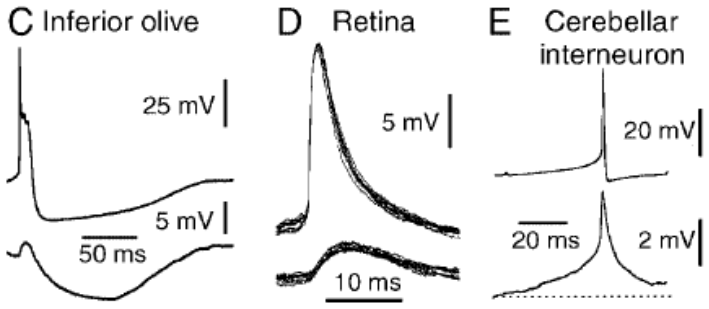


Figure 8: Examples of electrical coupling via gap junctions in different areas of the brain.

Numerous studies, both experimental and computational, have focused on analyzing the synchrony of neuronal networks connected via gap junctions [31, 41, 50, 56, 57, 60]. The computational work has involved a variety of cell types ranging from pancreatic beta cells to interneurons, and has been focused on analyzing coupling strength when changing gap junction connectivity or intrinsic currents within the cells [50, 56].

$$I_{GJ} = \sum_{j=1}^{C} g_{GJ}(V_j - V_i) \tag{8}$$

Equation 8 presented above shows the gap junction current $I_{GJ}$ that is received by neuron $i$ from the $C$ gap junction connections that it forms with other neurons, and is based on a classical model presented by Perez-Velasquez and Carlen [49]. Figure 9 shows an example of one of our models with two neurons connected by gap junctions.

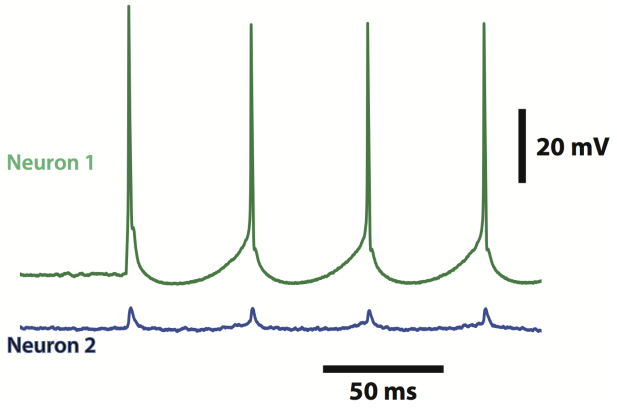


Figure 9: An input current of 1 nA was applied to Neuron 1 while no input current was applied to Neuron 2. Application of current to Neuron 1 elicits action potential firing in this neuron and changes in membrane potential in the gap junction-coupled neuron (Neuron 2).

## 2.4 Details of Creating the HM Network Model

As mentioned in section 2.2.1, the individual neurons were modeled using the ionic current equations from the rat hypoglossal motoneuron (HM) mathematical model generated by Purvis and Butera [52]. The parameters for the ionic currents of the cells were initially not changed from the Purvis-Butera model for the first study. Eventually, for one of our studies, we tested different levels of SK (small-conductance $Ca^{2+}$-activated $K^+$ channel) conductance.

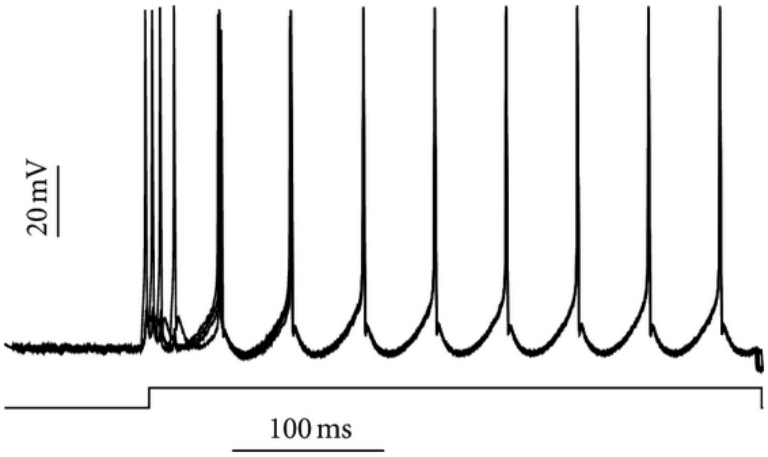


Figure 10: Example of four HMs connected with each other via gap junctions. The neurons rapidly attain perfect synchrony.

For our simulations, Euler's method was used for numerical integration with a time-step of 0.05 ms. A few of the simulations were checked at a dt=0.01 ms to ensure correctness and numerical stability. The usual input to the system was a square-wave excitatory current applied to each neuron at slightly different starting times (as seen in Figure 10 with the first spikes occurring at different times). A variable white-noise was added at every time-step. We have created homogenous

networks of hundreds of HMs probabilistically connected into a network via simple gap junctions. The implementation of the gap junctions was based on the model by Perez-Velasquez and Carlen [49] as described in section 2.3. A basic example of our model with four neurons connected with high-conductance gap junctions is shown in Figure 10.

### 2.4.1 Neuronal Synchrony

Synchronized neuronal activity can be associated with both healthy neuronal functioning and pathological conditions. Respiratory motoneurons require some degree of synchrony to coordinate intrinsic and extrinsic tongue muscles [4], diaphragm and tongue motoneurons [65]), and left and right hypoglossal nerve activities during respiration [48]. On the other hand, excessive synchrony, particularly through gap junction coupling, has been shown to be associated with seizures [49]. A major part of this chapter of the dissertation focuses on analyzing the synchrony of our network models, in particular under the effect of gap junction coupling.

$$\chi = \frac{\overline{(\frac{1}{N}\sum_{i=1}^{N} V_i(t))^2} - \overline{(\frac{1}{N}\sum_{i=1}^{N} V_i(t))}^2}{\frac{1}{N}\sum_{i=1}^{N}(\overline{V_i(t)^2} - (\overline{V_i(t)})^2)} \tag{9}$$

We needed an objective measure to make numerous comparisons and analyses for synchronized neuronal network behavior. To evaluate synchrony, we implemented a quantitative measurement of network synchrony that we call $\chi$ (Equation 9), originally proposed by Hansel et. al. [28]. This synchrony measure is computed by calculating the ratio of the time-averaged variance of the population voltage and the population average of time-averaged variance of single cell voltage. However, unlike the standard form, which is applied to data points over all time, for some of the studies we apply the measure to short time bins of 200-500 ms duration consecutively. Much like a short-time Fourier transform, this provides insight into how

the properties of the signal change over time and helps to ameliorate limitations of a method that was originally intended for use over the entire signal.

### 2.4.2 Using the Model

Our network model of HMs was used extensively to test aspects of gap junction coupling. In this dissertation, we present three of our most thorough studies. In our first study we performed an analysis of the effects of lowering gap junction conductance to address some conflicting observations from gap junction blockade experiments. In our second study, we analyzed the effect of changing the amplitude of the excitatory input current to HMs and the influence of specific ion currents (such as the $Ca^{2+}$-gated $K^+$ channels) on the synchronized behavior of a network of HMs with different gap-junction coupling conditions. In our third study, we analyzed an interesting emerging Central Pattern Generator (CPG)-like behavior under conditions of gap junction coupling, where the HMs divide themselves into different firing groups.

## 2.5 Study 1: Analyzing Gap Junction Blockade

In this study, we performed an analysis of the effects of lowering gap junction conductance to address some conflicting observations from gap junction blockade experiments.

### 2.5.1 Uncoupling Simulations

Blockade of gap junctions has been shown to alter respiratory activity by affecting inspiratory-phase neuronal synchrony [9, 60], an observation that is consistent with the idea that the conductance and opening or closing of gap junctions has a

direct effect on synchrony of neuronal networks [56]. Intuitively, one might assume that gap junction blockers would produce a complementary decrease in neural synchrony; however, studies examining the effects of gap junction blockade have produced mixed results. In the field of central respiratory control, this is highlighted by a series of studies focusing on respiratory rhythm generation and inspiratory-phase neuronal synchrony. In these studies, Solomon et. al. [60] demonstrated that pharmacological blockade of brainstem gap junctions reduces inspiratory-phase synchronization in the phrenic nerve in the adult rat while Bou-Flores and Berger [9] showed that on a short-time-scale, gap junction blockade increased inspiratory-phase synchronization in the hypoglossal and phrenic nerves in the neonatal rat. Additionally, Winmill and Hedrick [73] reported that fictive breathing was differentially affected by blockade of gap junctions in larval versus adult bullfrogs. While age-related differences in Cx expression and gap junction coupling are known to exist [1, 6, 12, 59, 61–63], it is unclear how or why neuronal synchrony would be differentially affected by blockade of gap junctions in the above studies. To address these curious and conflicting findings in the literature, we used our model of the network of HMs in the hopes of elucidating potential mechanisms that might explain the gap junction-mediated decreases versus increases in neuronal synchrony.

To simulate the gap junction blockade experiments, we first established a gap junction-coupled 100 motoneuron model. After simulating this model until full synchrony is achieved, gap junction conductance was gradually lowered, but never reduced to zero, since some of the pharmacological agents used to block gap junction coupling may only partially reduce channel conductance albeit other pharmacological agents completely close the channel (reviewed by Rozental et. al. [54]). A detailed example from these simulations is shown in Figure 11. As gap junction conductance decreases, so does neuronal synchrony. The decrease in synchrony is

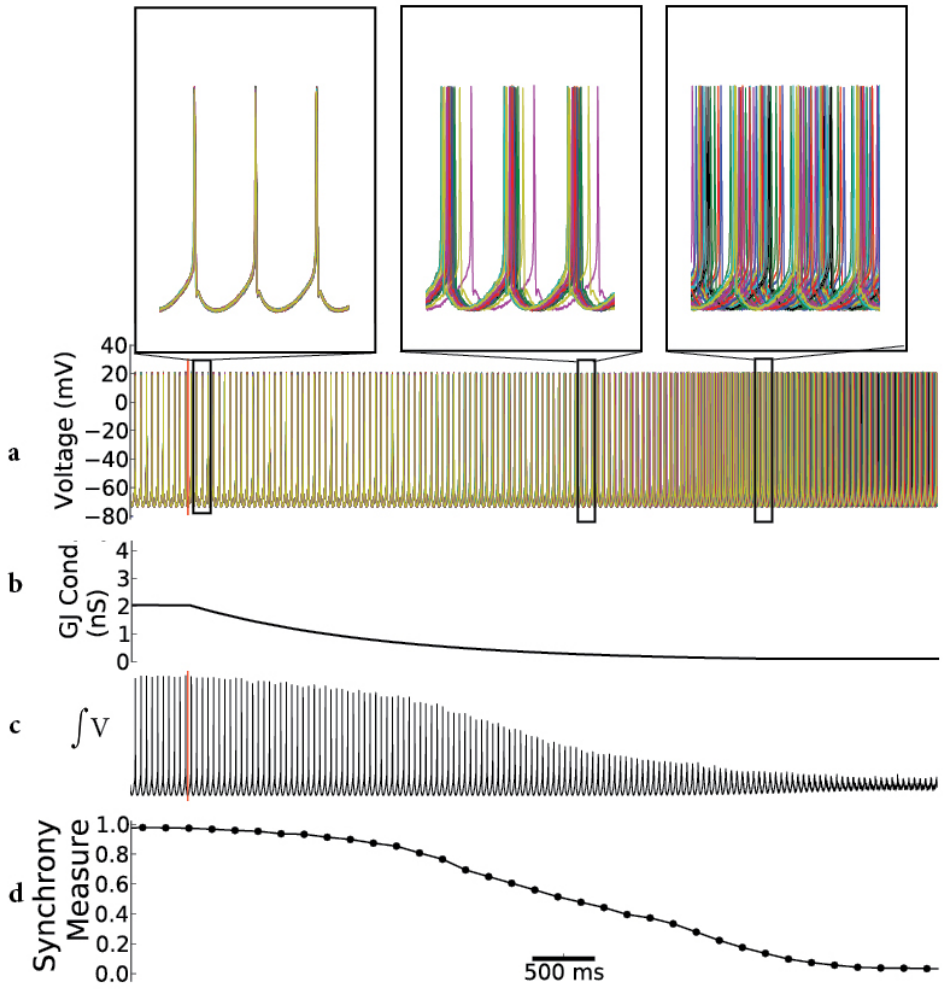


Figure 11: Example of simulation showing the effects of gap junction uncoupling. The biological simulated time was 8 seconds on a network of 100 motoneurons. (a) Voltage traces from a selection of 20 of the neurons; upper panel shows expanded traces from 3 regions indicated, demonstrating perfect synchrony during the initial segment, the reduction of synchrony as the neurons are uncoupling during the second segment, and unsynchronized firing in the final segment. (b) Average gap junction conductance (in nS). (c) Integrated total voltage trace of the entire network. (d) The measure of synchrony of the network with data points every 200 ms.

clearly seen when all voltage traces are summed together in part c of the figure, although the decrease in total voltage may not necessarily reflect a loss of synchrony.

### 2.5.2 Gap Junction Blockade of Motoneuron Nucleus and Upstream Inputs

Under experimental conditions in which the application of gap junction blockers is provided by bath application or systemic perfusion, the effects of gap junction blockade may not be exclusive to the neuronal population under investigation but could be influenced by other neural areas that provide direct or indirect input to this region.

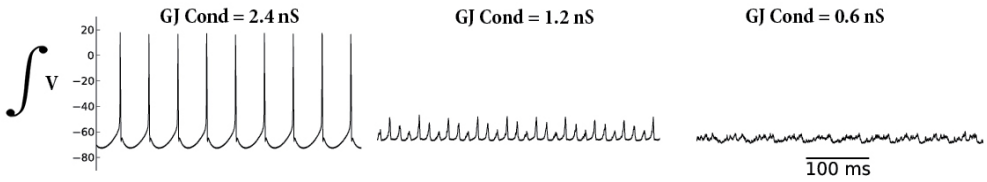


Figure 12: Lowering the gap junction conductance and resulting decrease in integrated voltage output.

In the respiratory circuit, for example, some respiratory-related neurons in addition to the HMs have been shown to exhibit gap junction coupling. This includes the pre-BotC [53], which is the primary locus of inspiratory activity and as such is the major component of inspiratory drive to which hypoglossal motor activity is entrained. Thus, a decrease in gap junction coupling in the pre-BotC, which is upstream of the HMs, could alter HM activity since blocking gap junctions would be expected to decrease the total voltage (Figure 12) from this region as well. If

this were to occur, it would lead to an alteration in the strength of the input to the HMs. To assess this possibility, upstream gap junction blockade was incorporated into the model as a reduction of the input current to the motor nucleus.

Thus, for these simulations, both the motoneuron nucleus and its upstream drivers were subjected to gap junction blockade by simultaneously reducing input current and gap junction conductance. Under these conditions, we observed effects that were distinct from those shown during gap junction blockade of the motoneuron nucleus alone (Section 2.5.1). In this case, rather than a decrease in synchrony, an increase in synchrony was observed as gap junction conductance was steadily decreased (Figure 13A). Concomitantly, the measure of neural synchrony was also increased, verifying that synchrony increases as gap junction conductance is reduced (Figure 13B).

To ensure that this effect is not an exotic behavior contingent on precise parameter settings, we ran several simulations over a broad variety of input currents and gap junction conductances. These simulations are summarized in Figure 14 and clearly demonstrate that synchrony increases monotonically with increases in gap junction conductance for a fixed input current and decreases monotonically with increases in input current for a fixed gap junction conductance.

Our simulations have demonstrated that gap junction blockade generally produces a decrease in neuronal synchrony when applied exclusively to the nucleus of interest and either an increase or decrease in neuronal synchrony when decreases in gap junction conductance and input current are combined. We suggest, however, that whether synchrony is reduced or enhanced potentially relies more heavily on the nature of the incoming inputs into a nucleus rather than froim a reduction of synchrony in the nucleus itself. Though gap junctions have traditionally been viewed as simple synchrony enhancers, and some of our simulations appear to support this view, our study has highlighted the idea that the role of gap junctions can be deeply

nuanced and highly dependent on the state of the cell and surrounding tissue.

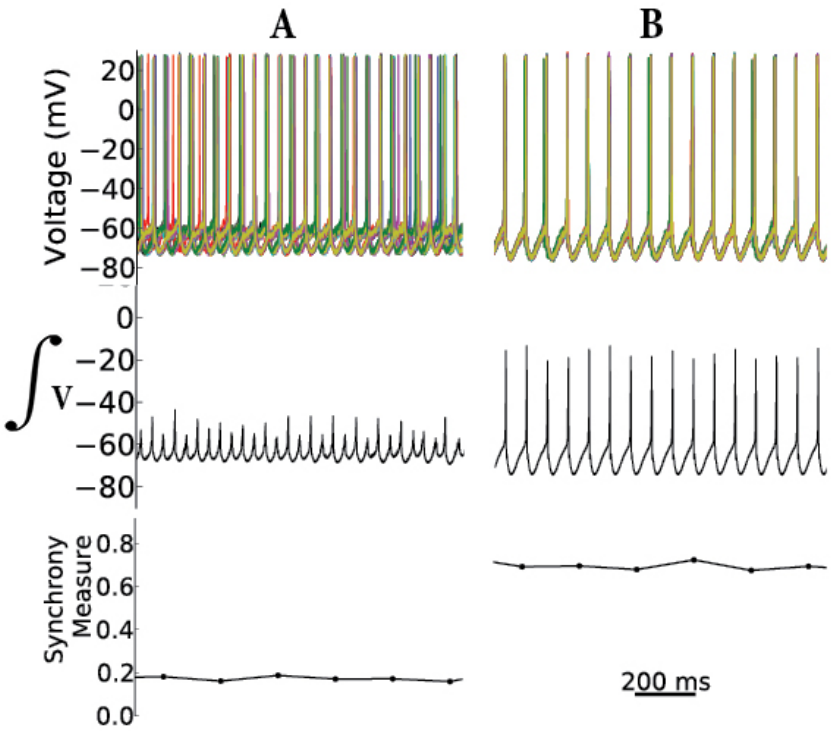


Figure 13: Reducing the input current (I) and gap junction conductance enhances neuronal synchrony. In (A) I=0.5nA and gap junction conductance = 1.2nS; in (B) I=0.3nA and gap junction conductance = 0.8nS.

While mixed results have been reported in the literature, the mechanisms underlying these differences were not identified. Thus, our simulations provide new mechanistic insight explaining these differences.

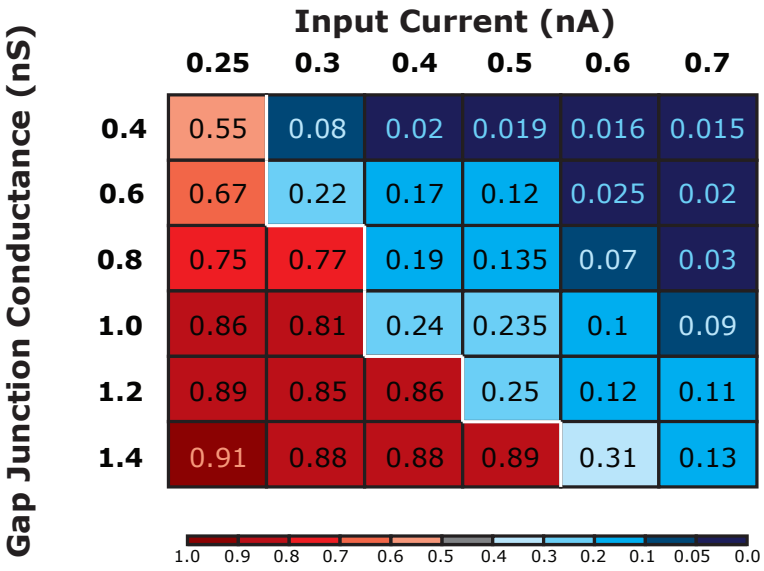


Figure 14: Effect of changes to gap junction conductance and to input current on neuronal synchrony.

It should be noted, however, that at the onset of this study, we did not expect neuronal synchrony to increase with simulated gap junction blockade. While our observations verify that an increase in synchrony can occur with gap junction blockade, it certainly defies intuition. Previous computational models of oscillatory networks have shown that while strong gap junction coupling can synchronize neuronal oscillations, weak gap junction coupling can phase-lock cells [42,57], the later of which could potentially lead to an increase in neuronal synchrony. An alternate explanation, however, must be considered when taking into account the methods employed for application of the gap junction blockers in the experimental studies described above. In this case, we reasoned that since the gap junction blockers were applied directly to the artificial cerebrospinal fluid bathing the tissues, they might have affected CNS areas other than the motoneuron nucleus responsible for

the motor output studied. If this were the case, the synaptic input to the hypoglossal and/or phrenic motoneuron nuclei would potentially be reduced. Assessment of this possibility revealed that simultaneously reducing the gap junction conductance and the input current that corresponds to the input from the upstream drivers can produce in an increase in neuronal synchrony, an effect that was distinctly different from that observed when reducing only gap junction conductance of the motoneuron nucleus. Thus, our computational model and simulations clearly demonstrate that gap junction blockade can decrease or increase neural synchrony depending on the circumstances associated with drug application.

## 2.6 Study 2: Effects of Firing Frequency on Network Synchrony

### 2.6.1 Introduction

As a follow-up to the previous study on gap junction blockade and inspired by its results, we decided to look deeper into firing frequency as a related factor that may affect network behavior. In fact, there have been very few studies that have analyzed the effects of neuronal excitability and firing activity on network synchrony. Synchronous oscillations occur over a wide range of firing frequencies in different brain structures [49, 66, 68] and the synchrony can be sensitive to those frequencies. In the locus coeruelus, for example, it has been shown that increasing action potential frequency of individual neurons reduces the synchronized activity of the nucleus. Additionally, Chow and Kopell [15] performed a complete modeling study on various aspects of electrical coupling and confirmed that driving current

(which affects firing frequency) causes the models (mostly pairs of integrate-and-fire neurons) to lose synchrony or fire out-of-phase. Firing frequency modulation is typically achieved by controlling the input current that is supplied to the neurons in simulation, and also by changing intrinsic properties of the model. Here we analyze the effects of both.

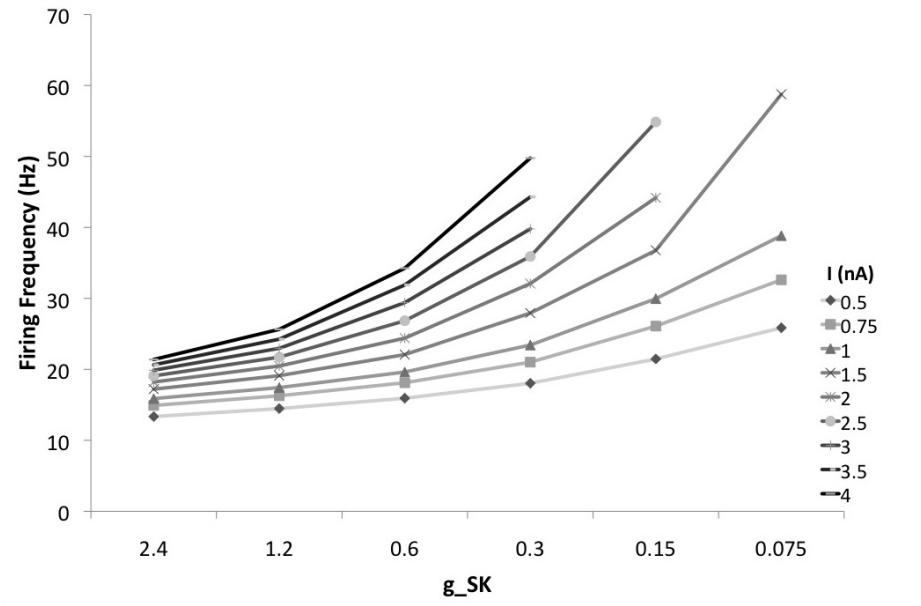


Figure 15: SK and firing frequency

Average firing frequency of a gap junction-coupled network in response to changes of SK conductance. Data shown were obtained from simulations with different levels of input current (as indicated).

### 2.6.2 Effects of SK and Input Current Amplitude on Firing Frequency

Firing frequency of neurons can be drastically influenced by changes in the parameters of specific ion channels. One of the typical ion channels that affects excitability,

is the $Ca^{2+}$-activated $K^+$ channel, also known as the "SK channel" [69]. SK channels are common throughout the CNS and are gated exclusively by intracellular $Ca^{2+}$ [53]. HMs are known to contain SK channels, and they play a role in both shaping the action potential as well as firing frequency [71]. We first examined how changes in SK conductance affect the excitability (i.e., firing frequency) of a neuron. For these simulations, SK conductance was altered for a fixed level of input current, and multiple levels of input current were evaluated. Figure 15 above illustrates the results of these simulations, and demonstrates that lowering SK conductance produces an increase in firing frequency at each level of input current tested.

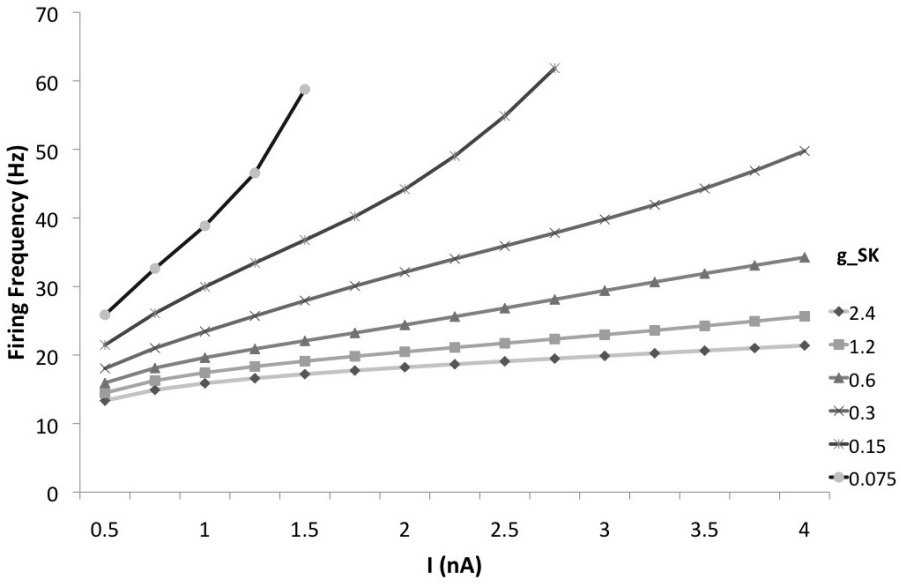


Figure 16: Average firing frequency of a gap junction-coupled network in response to changes in input current (I). Data shown were obtained from simulations with different levels of SK conductance (as indicated).

At the same time, it is well known that the firing frequency of neurons can also be modulated by the magnitude of the input current a neuron receives. So we also examined how changes in input current affect the excitability (i.e., firing frequency) of a neuron. For these simulations, an excitatory input current that ranged from 0.3 to 4 nA was applied. Similar to the above tests, for these simulations, SK conductance was set to a fixed level, and multiple levels of SK conductance were evaluated. Figure 16 illustrates the results of these simulations, and demonstrates that average network firing frequency increases in response to increasing the magnitude of the excitatory input current at each level of SK conductance tested. Gap junction conductance was set to a low level of 0.05nS for Figures 15 and 16.

Our simulations also revealed that firing frequency was significantly increased from a minimum of $\approx 10$Hz for the lowest level of applied input current to as high as 55 Hz for the highest level of applied input current, which is consistent with the range of "steady-state" firing frequencies reported for neonatal HMs [71].

### 2.6.3 Effects of Changing Firing Frequency on Synchrony

In order to perform a more thorough analysis of the effect of changing firing frequency (by changing SK and input current) on strength of synchrony, we decided to divide our simulations on gap junction-coupled networks with: (1) low coupling strength, (2) medium coupling strength, and (3) high coupling strength. The parameters chosen are presented in Table 1 and three typical examples from these simulations are shown in Figure 17.

Table 1: Parameters values for grouping simulations in three different levels of synchrony

| Category | Connectivity | Gap Junction Conductance | Synchrony Range |
|---|---|---|---|
| Low | 3% | 0.05 | <0.25 |
| Medium | 5% | 0.1 | 0.25-0.75 |
| High | 10% | 0.2 | >0.75 |

Using the two methods described above for altering firing frequency, we tested whether network synchrony is influenced by changes in firing frequency with the simulations divided in three different levels of coupling as described in Table 1. The results of these simulations are summarized in Figure 18.

Regardless of the strength of gap junction coupling, increasing firing frequency by either method generally produced an overall decrease in network synchrony, illustrating a clear anti-correlation between synchrony and firing frequency. Results from these simulations for both the effects of decreased SK conductance-mediated increases in firing frequency (Figure 18A) and increased input-current-mediated increases in firing frequency (Figure 18B) clearly illustrate this trend although the precise behaviors elicited by each method as well as under each coupling strength condition are somewhat different.

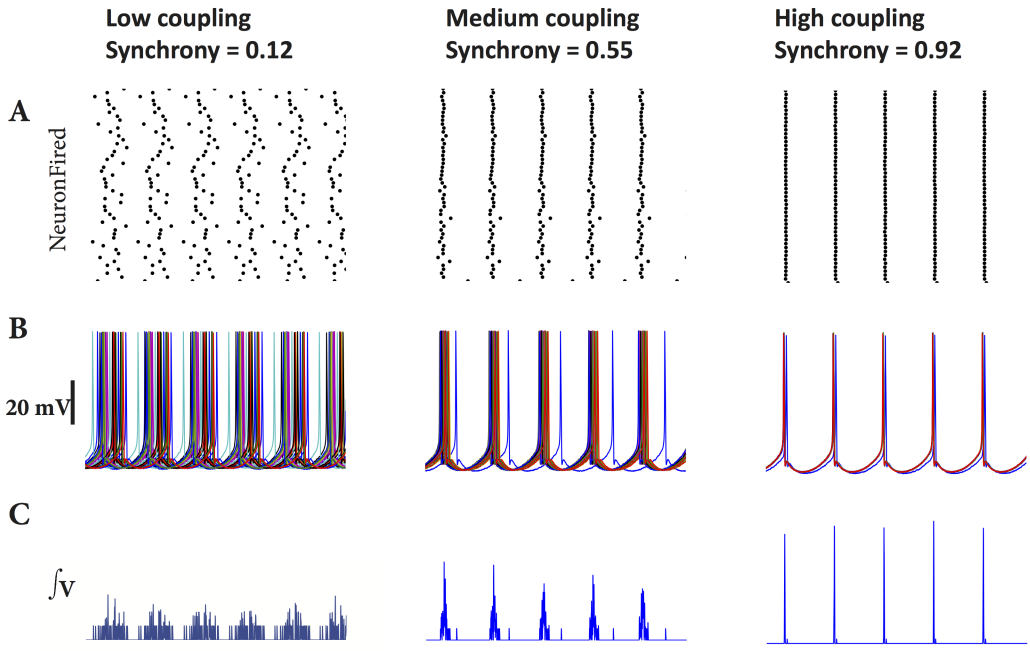


Figure 17: Three levels of coupling

While this trend was generally observed under all simulation conditions, it should be noted that the level of synchrony was (1) consistently below 0.3 in networks with low coupling strength (2) between 0.3 and 0.6 in networks with medium coupling strength, and (3) between 0.4 and 1.0 in networks with high coupling strength. Furthermore, regardless of the initial level of synchrony observed for the different levels of coupling strength, all networks were susceptible to changes in firing frequency. Moreover, in networks with both low and medium coupling strengths, firing frequencies of >20 and >30 Hz, respectively, were capable of reducing synchrony to near zero, indicating that the neurons in these networks essentially became fully desynchronized.

Our simulations also revealed some noticeable differences for the effects of

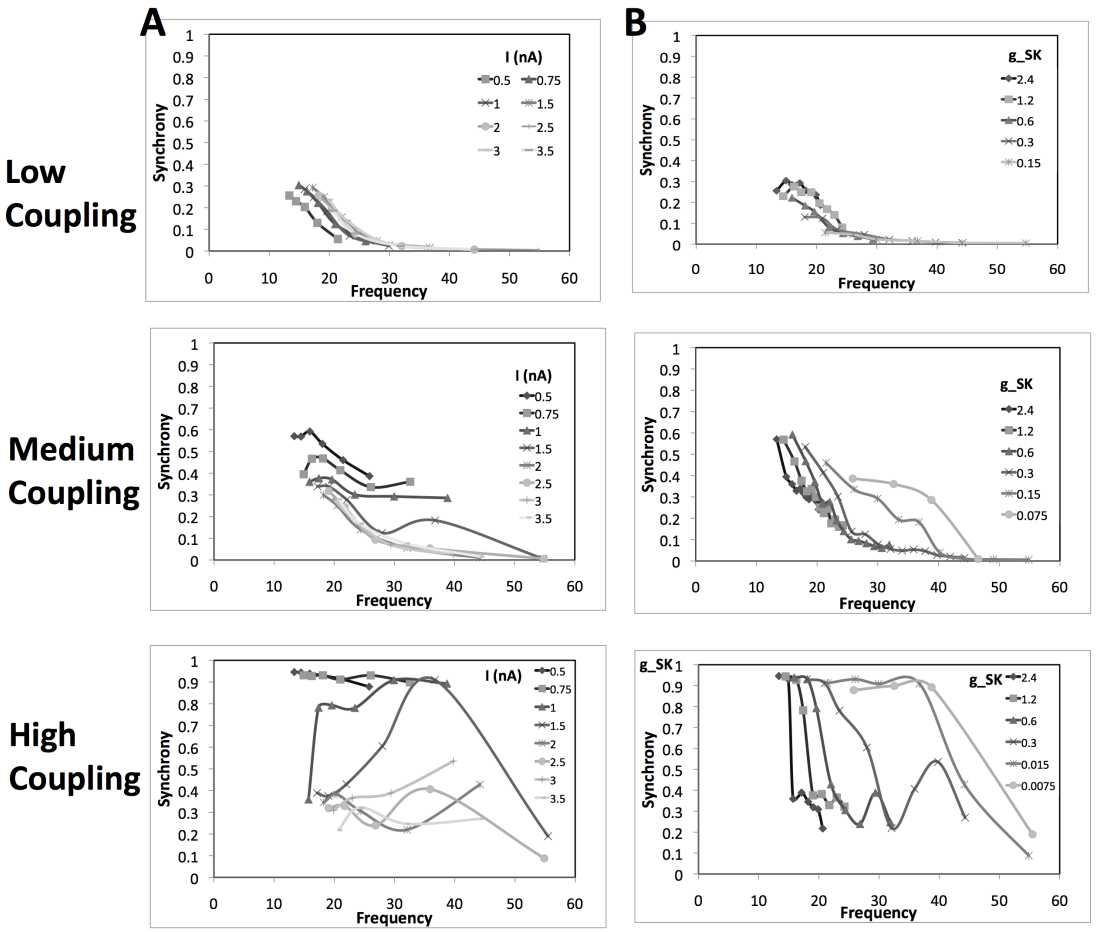


Figure 18: Synchrony in a gap junction-coupled network in response to changes in firing frequency for the three different levels of coupling strength. A. Simulations showing the influence of changes of SK conductance at different levels of input current. B. Simulations showing the influence of changes in input current at different levels of SK conductance.

SK conductance-mediated changes in firing frequency (Figure 18A) versus those for input-current-mediated increases in firing frequency (Figure 18B), especially in networks with medium and high coupling strengths. In networks with medium coupling strength, for example, decreasing SK conductance markedly increased firing frequency, but only elicited a slight decrease in synchrony; increasing input current modestly increased firing frequency, but produced a sharp decrease in synchrony. In addition, when input current was very close to rheobase with high levels of SK conductance, a small decrease in SK produced a very slight increase, rather than a decrease in synchrony.

Our simulations also revealed that networks with high coupling strength display the greatest degree of spread and volatility in synchrony. In these networks, two subtypes of network behavior were observed in response to SK conductance-mediated increases in firing frequency: (1) networks that exhibited a high level of synchrony ($\approx 1.0$), but became slightly less synchronized as SK conductance was decreased and (2) networks that exhibited a moderate level of synchrony ($\approx 0.4$), but became more synchronized as SK conductance was decreased. In contrast, input-current-mediated increases in firing frequency elicited more consistent behaviors. In this case, with low levels of input current, synchrony remained very high, and as input current was increased, synchrony dropped either gradually or abruptly. During these steep drops, slight increases in firing frequency occasionally elicited an increase in synchrony, which was followed by a continued precipitous decline. Additionally, in some networks, a high degree of synchrony was maintained even at relatively high firing frequencies although at the highest firing frequencies, a decrease in synchrony was observed [21]. These findings could potentially be reconciled based on the previous study presented in this dissertation, indicating that gap junction blockade can produce varying effects, from increased to decreased synchronization, depending on whether or not upstream premotor neurons are also

affected by gap junction blockade [41].

Additional simulations were performed to examine the effects of firing frequency changes on gap junction-coupled networks with extreme values. In this case, a network that was almost completely unsynchronized (with very low gap junction coupling) and a network that was almost perfectly coupled (synchrony above 0.98) were used. Our simulations in the unsynchronized network revealed that increasing firing frequency was ineffective in producing any significant changes in synchrony (not shown). Similarly, our simulations in the almost perfectly coupled network revealed that synchrony was not disrupted by increases in firing frequency (not shown). We interpret these observations to suggest that extreme values for gap junction coupling seem to protect against frequency-based changes in synchrony.

While both decreasing SK conductance and increasing input current increased firing frequency, which tended to reduce synchrony, each method for modifying firing frequency and synchrony did so at a different rate. While changes in input current greatly altered synchrony with small changes to firing frequency,changes in SK conductance tended to produce larger changes in firing frequency with less pronounced changes in synchrony (as seen by the less steep curves in 18A). Though it is not entirely clear why changes in SK conductance and input current have these particular effects, we speculate that it has to do with the dual effect of SK on firing frequency and spike shape, as compared to the single effect of input current on firing frequency alone. In this case, altering spike shape simultaneously with firing frequency may help to maintain synchronization when it would otherwise be lost.

## 2.7 Study 3: Emergence of Multiple Firing Groups

### 2.7.1 Introduction

During our simulations, we noticed an interesting emerging property of the firing activity of the neurons. Despite no explicit division of neurons into two groups, we observed a spontaneous division of neurons into two distinct firing groups, as in the example shown in Figure 19. This behavior resembles models of central pattern generators (CPGs). Central pattern generators (CPGs) are observed in neural regions that spontaneously generate oscillatory behavior in the absence of patterned input. In both invertebrates and vertebrates, they appear to play a critical role in the formation of repeated oscillatory behaviors, including activities such as walking, swimming, heartbeating, and breathing [13, 38]. Because of their roles in cardiac and respiratory function, CPGs may be considered vital for basic survival across much of the animal kingdom.

Traditional CPG models usually involve two distinct nuclei mutually inhibiting one another via synapses. Our model is very different since it is only a single nucleus model with random gap junction coupling. The division of the neurons into multiple firing groups appears sensitive to gap junction conductance, probability of gap junction coupling between cells, topology of gap junction coupling, and, to a lesser extent, input current into our simulated networks.

Traditionally, reciprocal synaptic inhibition between two neuronal populations (or two groups of neuronal populations, or even two individual neurons [55]) is seen as the standard method of generating CPG behavior in both biological and computational systems. Originally proposed by Brown [11], this style of CPG appears in biological models of lamprey and mammalian locomotion models [40] and as a component in more complex models of respiratory activity [58]. This form of CPG

is often referred to as the half-center model and is a prominent model for robotic locomotion controllers.

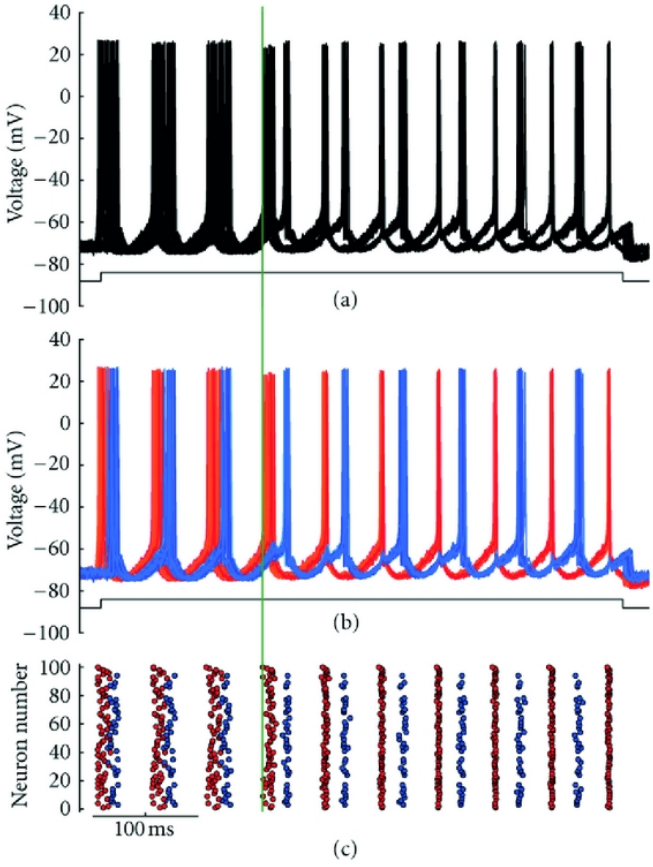


Figure 19: Emergent firing groups

While half-center CPGs typically focus on synaptic inhibition, recent work indicates that gap junction coupling may also play a role in locomotor patterns [36] and respiratory patterns [53, 60]. A combination of gap junctions and synaptic inhibition may also be responsible for synchrony in some neuronal populations, and even if gap junctions are not responsible for generating a mutually inhibitory connection, inhibitory currents coupled by gap junctions could easily play such a

role [67].

Although hard-wired reciprocal synaptic inhibition may be easy to identify physiologically, we propose that this same style of inhibition can spontaneously form in a single pool of gap junction-coupled neurons, mutually inhibiting one another via their slow afterhyperpolarization (sAHP). The sAHP following the action potential can be modified directly through $Ca^{2+}$-gated $K^+$ channels e.g., via the $I_{SK}$ channel as shown in the previous study, that are known to play an important role in burst frequency modulation. Since neurons would dynamically assign themselves to one of the two "half-centers", changes to gap junctions or inputs alone could modify how individual neurons align their firing. This would produce a highly dynamic modifiable half-center CPG capable of adapting to the rapid demands of locomotion or respiration.

Table 2: Total connections in firing groups

| Category | From group 1 | From group 2 |
|---|---|---|
| Connections to group 1 | $CS_1(S_1-1)/2$ | $CS_1S_2/2$ |
| Connections to group 2 | $CS_1S_2/2$ | $CS_2(S_2-1)/2$ |

Here, we present a biologically realistic model of gap junction-coupled neurons that exhibit multiple output rhythms typical of half-center CPGs. Unlike standard half-center CPG models, however, we have one pool of ubiquitous neurons with random gap junction coupling that are still able to output two or more distinct phase-shifted rhythms.

### 2.7.2 Half-Center-like Behavior

In the simulations, following the opening of gap junctions, two distinct phase-shifted signals reminiscent of a traditional half-center CPG could be generated in a single nucleus with ubiquitous connectivity. An example of this behavior is shown in Figure 19, where opening the gap junctions shifted a fairly asynchronous firing pattern among the 100 neurons into two distinct neuronal firing groups. To highlight this division into two firing groups, the neurons were color-coded according to their group affiliation (Figure 19(b)). A raster plot of their spiking behavior was also generated Figure 19(c). In general, one group was often better aligned than the other, and upon further investigation, the randomness and ubiquity of connectivity actually fostered conditions encouraging one slightly larger group to act as a "driver" for the smaller "follower" group. On average, connectivity between and within the firing groups is given in Table 2, with the probability of two neurons being gap junction-coupled set to C, and the number of neurons in firing group i being $S_i$.

Table 3: Fraction of connections in firing groups

| Category | From group 1 | From group 2 |
|---|---|---|
| Connection ratio to group 1 | $(S_1 - 1)/(S_1 + S_2 - 1)$ | $(S_2)/(S_1 + S_2 - 1)$ |
| Connection ratio to group 2 | $(S_1)/(S_1 + S_2 - 1)$ | $(S_2 - 1)/(S_1 + S_2 - 1)$ |

While this implies that both groups are sending roughly an equal amount of

conductance between one another, as would be expected by bidirectional gap junction coupling, it masks a more important property. Since each group has a very different degree of interconnectedness, the amount of incoming drive in relation to internal drive is markedly different (see Table 3).

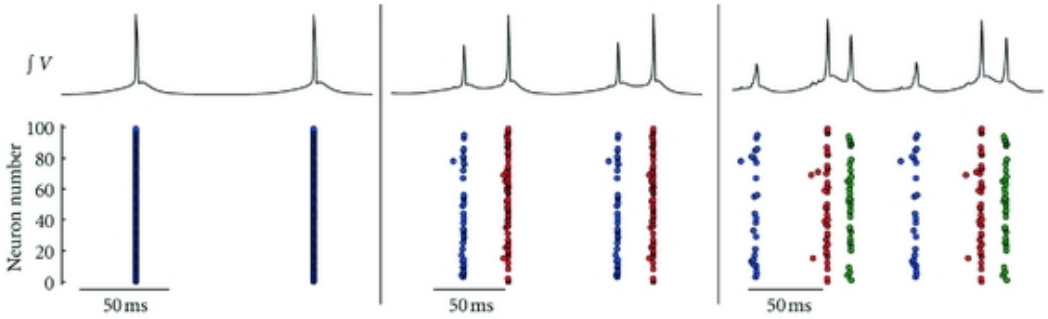


Figure 20: Three firing groups

As $S_1 > 1$ and $S_2 > 1$, the ratio of internal connections in group 1 is identical to the ratio of connections in group 2 received from group 1. Regardless the size of each spontaneously formed group, the larger group always receives more internal than external stimulation and extends more excitability to drive the smaller group. Thus, based on probability alone, a similar topology is consistently observed regardless of network size. This does not exclude the possibility of having two equally sized groups, which would be expected to have more balanced dynamics. While the main focus of the current investigation is on half-center like CPGs, it should be noted that generating more than two groups is feasible even though more rare. In the model below, for example, three groups were observed (Figure 20).

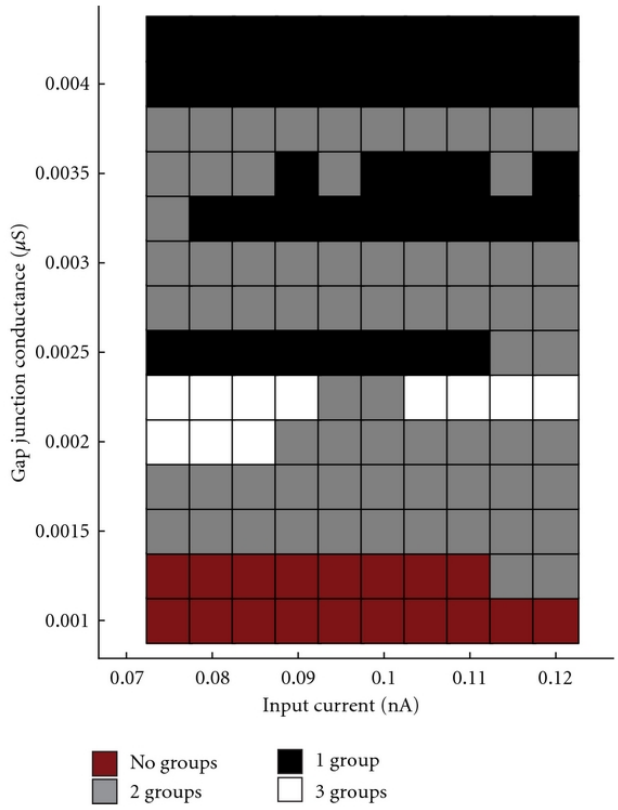


Figure 21: Gap junction conductance vs. input current

Furthermore, in a similar fashion with the previous two studies, we also looked at the effect of changes in input current amplitude. The results showed that even without altering patterns of connectivity, modifying conductance through gap junctions and/or input current into the system had the potential to shift the firing patterns between 1, 2, and 3 independent groups (Figure 21). In this case, gap junction conductance was seen to exert a greater influence than that of input current in determining the number of firing groups 21, with higher gap junction conductance being associated with fewer groups and lower gap junction conductance being associated with more groups. While input current was capable of producing a shift between

different firing behaviors, changes in input current were less predictive of a trend in the number of firing groups.

### 2.7.3 Topology Effects

Up until now, all of our models have used random connectivity without any concern for spatial placement of the cells. Since slice preparations are commonly used to study CPGs of the spinal cord, and the slice itself often has a thickness (350 - 600 $\mu$m) within the range of the dendritic span of motoneurons (250 - 700 $\mu$m), where gap junctions primarily form between dendrites and/or somas, we opted to orient neurons along a two-dimensional plane as a first approximation to this layout to begin to explore the effects of spatial connectivity on half-center like CPG group formation. Gap junction connections were made at random, with each cell having a probability of 50% of connecting to any cell within a radius of 5 in the model with topology. Neighboring cells in the plane topology were all evenly spaced in a square lattice, with non-diagonal neighbors at a distance of 1.

While one might predict that neurons in each firing group would clump together into two massive nuclei, this is not the case. Instead, neuronal groups tended to form a mottled appearance, with clumps from each group equally interspersed (Figure 22). This configuration would ensure that each neuron would be exposed to some members of each firing group, thus loosely preserving connectivity reminiscent of a topology-free model. Figure 22 also reveals that one neuron spent five firing cycles with the firing group color coded in red before joining the firing group color coded in blue. This suggests that unlike in a traditional half-center CPG where group allegiance is a hard-set property of each neuron, in some rare instances, a neuron may straddle the fence and move between two groups.

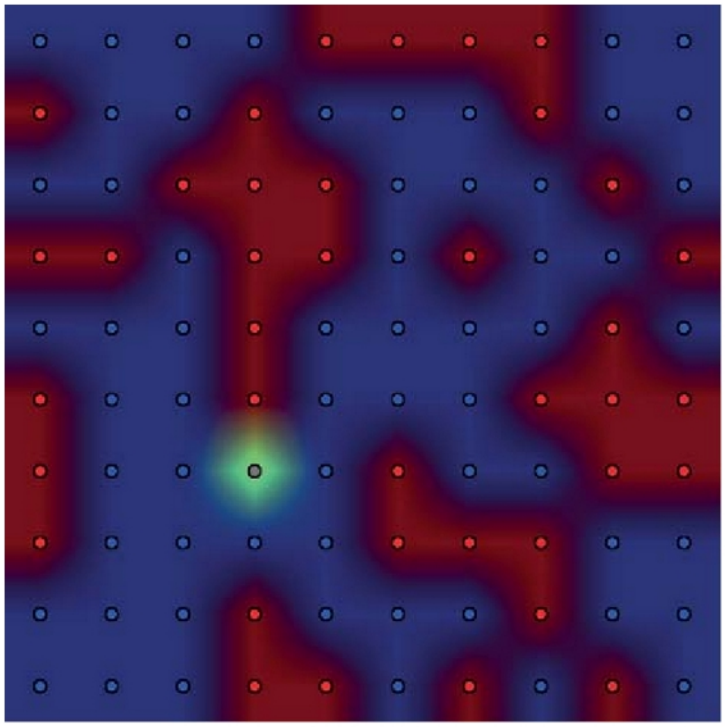

Figure 22: Mottled topology and firing groups

For Figure 23 multiple simulations were performed varying both the probability of forming a gap junction with a neighbor within a given radius and the radius itself. The results from this series of simulations resemble Figure 24, a plot based on the average of the total hypothetical conductance received by each neuron.

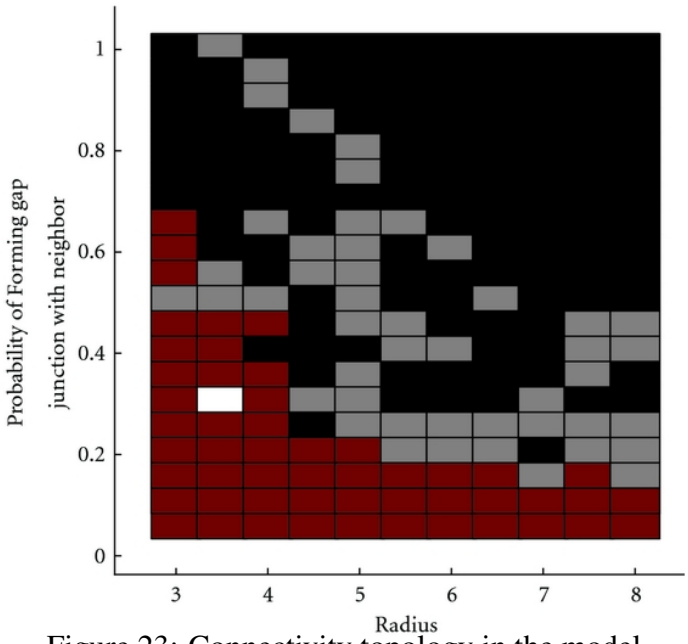


Figure 23: Connectivity topology in the model.

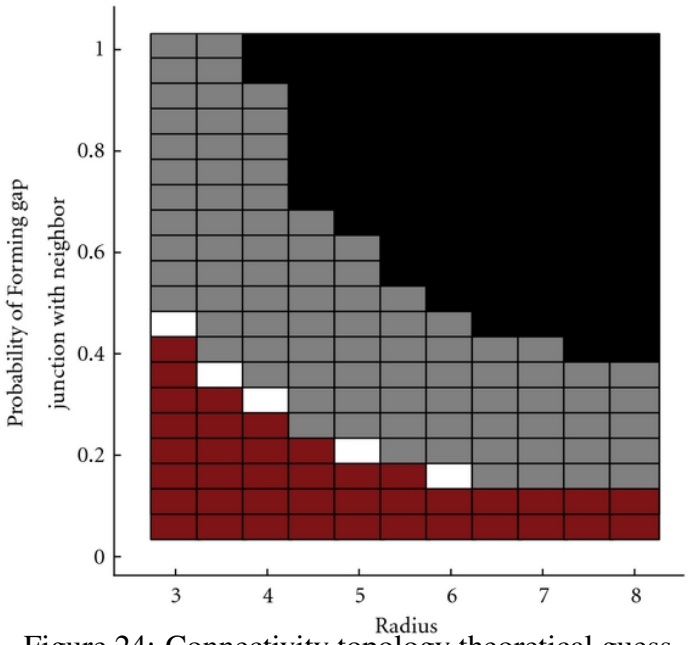


Figure 24: Connectivity topology theoretical guess

### 2.7.4 Discussion and Other Considerations

The dynamic nature of these CPGs would be especially beneficial for either the generation or modification of locomotor or respiratory central patterns. In contrast to our model, most models of CPGs incorporate static group affiliation, which alone may not be able to produce the sorts of dynamically changing locomotor and respiratory patterns seen in nature. In both locomotion and respiration, adaptation of rhythms to both external environmental changes and descending cortical commands may be more difficult in a simpler CPG, which may lack the requisite complexity required to describe the wealth of patterns that humans and other mammals are capable of exhibiting in these two activities. Moreover, CPGs formed through gap junctions can alter group affiliation without relying explicitly on changes in gap junction coupling. With this in mind, some of the rarer behaviors seen in the current model, including the more exotic three firing group behavior, might be easy for a biological system to generate and maintain as long as the initial state of the system is within the vicinity of the correct set of parameters. Evolutionarily speaking, it would also be easier to create a CPG that itself had no explicit wiring, but could rely on random connectivity to self-organize.

Though this novel CPG has many admirable traits, some inherent properties of these systems may make them harder to tune or more difficult to find biologically. The volatile nature of a system that drastically changes behavior with small changes in parameters could open such neural systems up to a plethora of neurological disorders. While we offer no strong hypotheses regarding known disorders that might stem from such a disruption, known disorders with errant or absent patterns certainly come to mind: spastic gait, persistent muscle spasms, and the sudden loss of breathing implicated in SIDS. Furthermore, because such systems can exist in a singular nucleus with otherwise ubiquitous physiological properties, the only way

to identify such systems experimentally would be to observe them while active, rather than through simple histology alone.

## 2.8 Other Studies, Considerations, and Limitations

Apart from the three studies described above, our work with networks of HMs has included other related topics, some of which can be analyzed in future studies. These topics include: creating and using a reduced model of the HM, analyzing network-level behaviors for the reduced model, analyzing developmental changes of HMs by creating subtypes of the model with different parameters for different age groups.

### 2.8.1 Reduced Model of HMs

We have developed a simplified model of the HMs, without many of the detailed ion channels of the Purvis-Butera model. The reduced model is a combination of the simple spiking Izhikevich [34] model, which contains only a $Na^+$, $K^+$, and leak current, with some additional channels. More specifically, it involves a voltage-gated $Ca^{2+}$ currents $I_{Ca}$, and the AHP (AfterHyperPolarization) current. The firing pattern is similar to the original model, as shown in Figure 25 below.

One of the reasons for creating the reduced model was to see if the simulations would run significantly faster on the reduced model, which has less than half the number of differential equations compared to the full model. But for large networks of neurons, the performance is very much influenced by connectivity, so even though the reduced model runs faster, the difference is not significant enough for networks of hundreds of neurons which contains many thousands of gap junctions. Figure 26 shows an example of performance difference in a network of 1700

neurons.

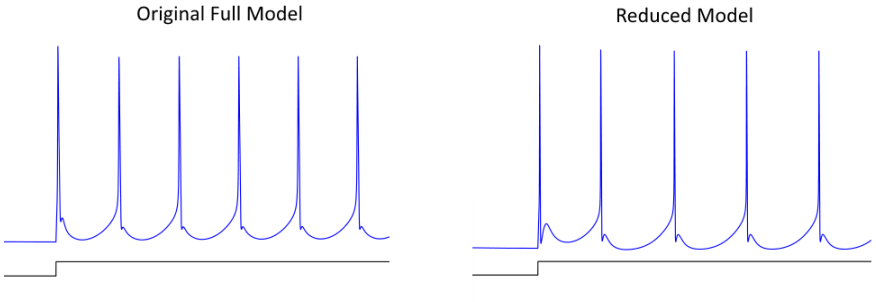


Figure 25: Full vs. reduced HM model firing behavior.

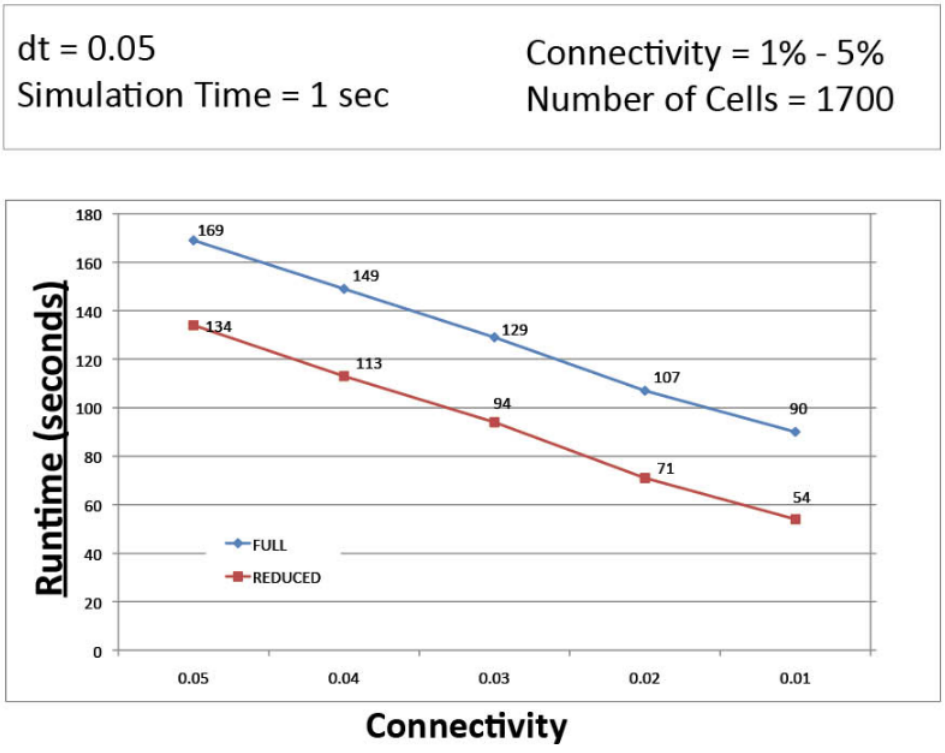


Figure 26: Performance (runtime) of full vs. reduced HM models in a large network

We even used the reduced model to analyze some of the behaviors from our

studies presented earlier in this chapter to see if some of those behaviors could be replicated. For instance, the CPG-like behavior with multiple firing groups (one, two, or three) can be reproduced in the reduced model as shown in Figure 27.

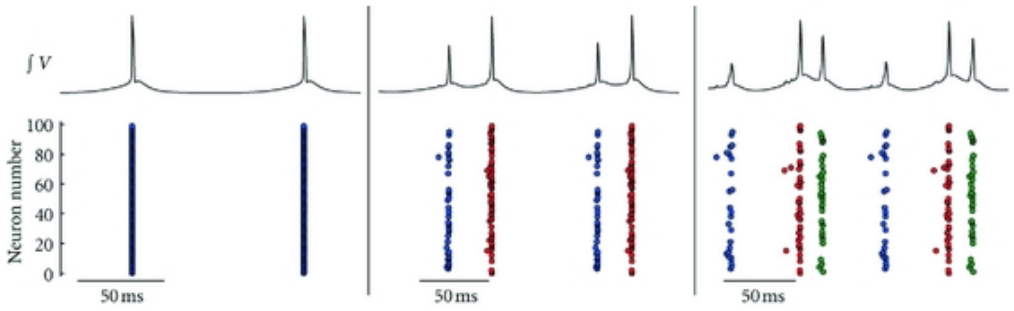


Figure 27: Reduced HMs displaying emergent firing groups behavior.

### 2.8.2 Subtypes of HMs

It is known that throughout development, HMs exhibit a variety of electrophysiological changes. The model that we used for our studies reflects the neonate electrophysiology. In our lab, we extended the initial HM model and have also created subtypes to reflect developmental changes. These changes were implemented by varying BK channels, and the $Ca^{2+}$ currents (both voltage-gated and leak). The firing frequencies of the HMs are quite different. There is also literature that demonstrates changes in the density of gap junctions with age. Interesting modeling studies with a developmental focus can be performed and all the studies mentioned above could be also analyzed from a developmental perspective but that is beyond the scope of this dissertation.

### 2.8.3 Limitations

The nature of computational models brings limitations that have to do with simplifying assumptions and incomplete knowledge of the systems that are being studied. For instance, as is common in modeling studies, the input currents chosen for the excitatory drive of the motoneurons are simplified and may not replicate the synaptic input received from the premotor nuclei. Despite the fact that the HM model that we used for these studies is a very detailed and thorough biophysical model, it still makes simplifying approximations such as treating the neuron as a single compartment and keeps track of only one value for a uniform membrane potential on the whole neuron.

As is the case with all modeling, a reasonable computational model does not necessarily imply the existence of a biological correlate. In addition, testing some of the guesses or conclusions made from our models may be extremely difficult to do experimentally in live animals. Furthermore, we are limited to the sets of parameters explicitly examined, and, therefore, we cannot rule out that additional mechanisms may play a role in those behaviors.

When modeling networks of neurons, we focus only on the neurons themselves. However, neurons do not exist in isolation, they are part of a tissue that involves many other cell types and the conditions of the tissue itself may affect neuronal functioning. Experiments like blockade of gap junctions in the biological situation may also affect the glia, which are known to contain extensive gap junction coupling [20], and the uncoupling of glia could contribute to behaviors in the system that we were not capable of capturing with the present model. It would be of considerable general interest to model the extent to which such coupling strength between an excitable neuron and a nonexcitable glial cell might affect neuronal network activity [43], and future studies could consider that possibility.

# Chapter 3

# BOSS and a Large Cerebellum Model

## 3.1 Introduction to the BOSS Project

Several research groups, rather than focusing on precise details in individual neurons, seek to build networks that consist of millions or even billions of neurons to reach scales where mass neuronal effects such as memory and visual perception emerge. Simulating large-scale neuronal models gives researchers the power to manipulate features of simulated neural tissues and observe both local and global properties of neural systems. During the last decade, large-scale brain modeling has risen in prominence, with a wide range of publications on brain-scale models [2, 33, 37].

Most large-scale modeling research groups focus either on networks that are highly realistic down to the individual axon collaterals and dendrite branches of each neuron, with the typical example being the Blue Brain project [39] or on systems that are simplified and run on massively parallel hardware, with the typical example being the Gordon Bell prize-winning model of a cat brain [2].

Rather than emphasizing biophysical or neuromorphic details, our group is more interested in a balanced approach that capitalizes on general structural connectivity and approximations of neuron morphology while trying to maintain the

overall behavior of the tissues as a whole. The Brain Organization Simulation System (BOSS) is the main ongoing project of our lab. It is a unified system for creation, simulation, and visualization of large-scale models of brain structures.

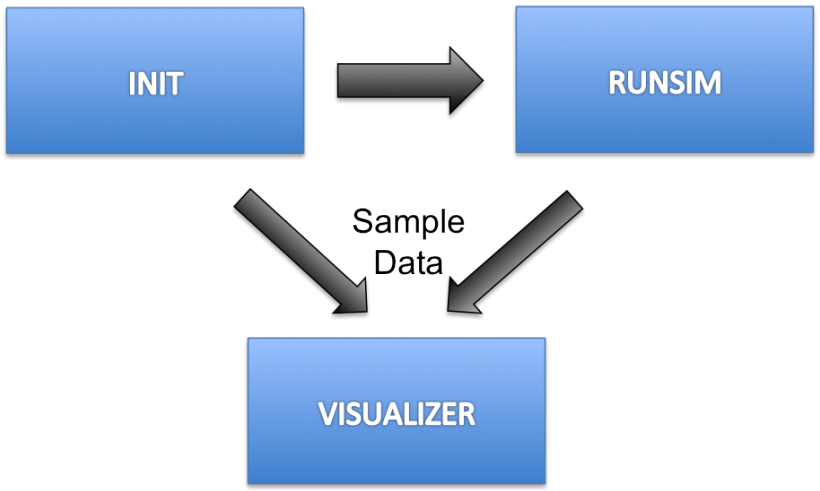


Figure 28: The BOSS project

As illustrated in Figure 28, the project consists of three major components:
INIT - an initializer in which parameters control the creation of the models;
RUNSIM - an efficient simulation engine;
VIZ - a custom visualization program.

We have continuously improved our tools making them more efficient and adding various features to make the models as accurate as possible. The modeling software gives identical results, except for timings and limits on model sizes, when run on a single laptop, a lab personal computer (PC), or on NY-Blue, the regional IBM Blue Gene supercomputer.

### 3.1.1 The Model Initializer: INIT

In the initialization phase (INIT), parameters specify spatial distributions of neurons and synapses and control creation of models that are morphologically representative neuronal networks. At the start of model creation, instances of all neuron types are placed in a three-dimensional (3D) simulation space. Axonal and dendritic fields, where all synapses are located, are approximated as 3D rectilinear boxes, as illustrated in Figure 29.

Synapse placement is of great concern in large-scale models, since synaptic connection patterns control the flow of excitation and inhibition through a neuronal network. A typical approach to initialize synapse placement is to prespecify a few pools of interconnected neurons and define the random likelihood that any two neurons in a given pool are connected by a synapse [3].

Rather than specifying neuronal pools, our approach draws from both statistical connectivity and spatial location mappings. Instead of defining neuronal pools without any sense of spatial geometry, we place neurons in 3D Cartesian (XYZ) space. Each neuron has axonal and dendritic synaptic regions at preset positions relative to its soma. We let each neuron form connections with other neurons within 3D overlap volumes of their synaptic regions. In this way, synapse locations are based on the spatial proximity of axons and dendrites by a method that is more detailed than placing synapses between randomly selected neurons, but less detailed than finding them where precise axonal and dendritic arborizations touch [39].

Our approach to building brain models starts with the creation of detailed parameter specifications. The program reads in a parameter file that statistically describes the neuronal and synaptic configuration of the brain tissues to be modeled. The parameter file can be either in plain text format or in an XML format with our predefined parameter namelists. Our program can be easily modified to accept input

files in other formats, such as neuronal description parameters in NeuroML [26].

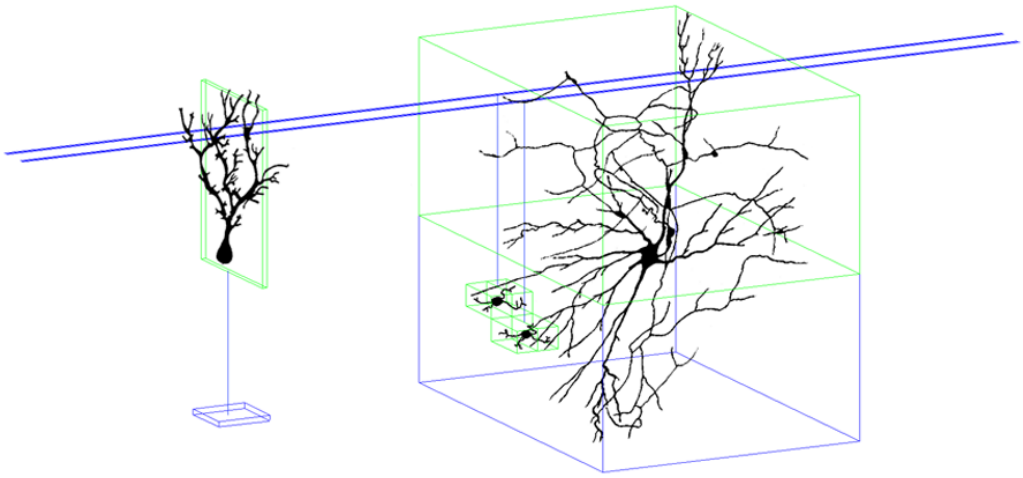

Figure 29: Three cell types of the cerebellum and the boxes representing their neuritic fields

The input parameter file contains a list of cell types, what pairs of cell types can form synapses, the density of each type of soma in the model space, the axonal and dendritic shapes and positions relative to the soma of each instance of a cell type, plus statistical properties about synapse concentrations and whether they are inhibitory or excitatory. See subsection 3.3.1 on building the cerebellar model for more details. The distances of each synapse from its axonal and dendritic somas combined with parameters specifying propagation speeds in axons and dendritic speeds at different distances from the soma determine propagation delays and attenuations for action potentials passing though each synapse. To lessen computer memory needs and execution times, our present modeling system does not consider branching details within dendritic trees.

After parsing the input file, the program places all cell instances in the 3D

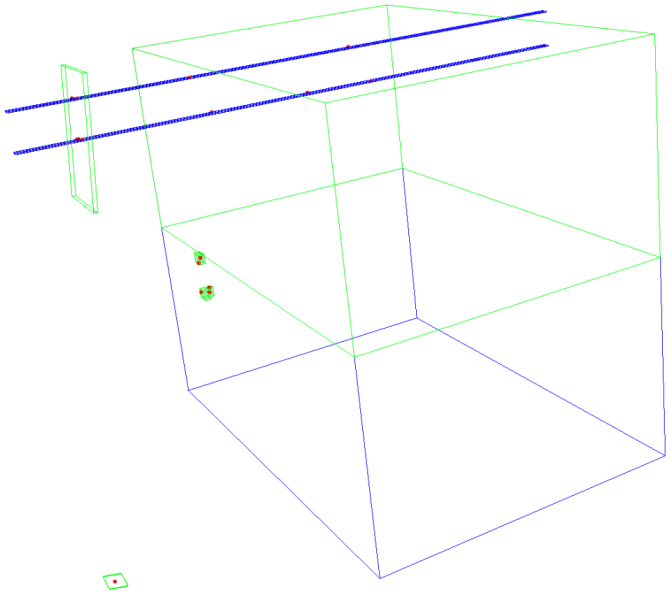

Figure 30: Bounding boxes

space. The axonal and dendritic regions, where all synapses are located, are approximated as axis-aligned bounding boxes (AABBs), as seen in Figure 30. All instances of neurons of the same type have their synaptic region boxes in the same positions relative to the soma, or cell center.

The most critical step for our approach is determining axonal-dendritic intersections once all volumes of potential connectivity have been specified by placement of all neuron instances. The task requires walking through three-dimensional space and determining where axonal and dendritic synaptic volumes overlap. For neuronal simulations involving many millions of neurons, finding overlapping volumes poses a significant computational challenge.

To perform neurite-overlap detection efficiently, we have developed a practical

algorithm to walk through the axonal and dendritic volumes. There are two variants of the algorithm: one "Staggered Walk" (SW) that performs the walk blindly in one predetermined dimension (e.g., X) and the other "Staggered Walk Dynamic" (SWD) that uses a quick method to determine the optimal dimension (X, Y, or Z) for starting the staggered walk [75]. These walk approaches turned out to be particularly useful in the rapid determination of connectivity between millions of neurons in moderate-scale to large-scale models. The algorithm starts by sorting the neuritic boxes in the predetermined same axis and then performs a plane sweep while maintaining lists of "open" and "closed" local boxes that may overlap. Once the code has walked past the "closed" points of neuritic fields, they are not considered anymore in the overlap comparisons. This saves a lot of computation time. Once an overlap is found, the algorithm calculates the volume of overlap and creates synapses based on the percentage of maximum possible overlap. Staggered walks provide an automated method to create verifiable simulation models by reproducibly specifying details of neuron placement and synaptic connectivity. Our algorithm scales well and within a few minutes permits the rapid creation of models containing billions of synapses, which would take many hours with a naive $O(N^2)$ approach.

### 3.1.2 The Simulator: RunSim

After all the structures get initialized, the run simulation (RunSim) phase begins. Our simulations use the Izhikevich integrate-and-fire models [34] that were described in the Introduction, Chapter 1. The Izhikevich model was chosen for its simplicity, computational efficiency, and flexibility in producing different behaviors with only a few parameter changes [34]. Since we are more interested in global large-scale network activities, we believe that we are not losing much by not having

detailed ion channels, as used for the Hodgkin-Huxley style neuron models.

Our models run not only on standard PCs, but also on supercomputers with identical results except for timings and model size limits. We have used up to 1024 nodes on a Blue Gene/P, and up to 4096 computing nodes on a Blue Gene/L. We use MPI (Message Passing Interface) for the parallelization of the code across nodes. [27]. We call our model space a "universe" and the Cartesian space is divided equally into "nodes". Each node is responsible for all synapses within its zone that provide dendritic inputs to somas located in its node space. The "zone" is a region surrounding each node's portion and includes any data pertaining to cells connecting to neurons in that node. We have also added multithreading via OpenMP to get performance improvement when the code runs on multicore architectures.

During simulation runs, model time is divided into equal time steps. Euler's method is used for the numerical integration to calculate the voltage V in the Izhikevich model for each neuron. After each time step, lists of neurons that have just fired are broadcast among all computing nodes. Nodes receiving firing signals adjust synaptic weights and neuronal excitation levels as needed. We have implemented an image filter mechanism, where the pixel levels of an image get transformed to probabilities of force firing neuron types (in most of the cases the mossy fibers).

Model sizes are limited primarily by the amount of computer memory available to hold synapse data at runtime. The reason is that there are many more instances of synapses than any other data structures (such as neuron somas, neuritic fields). We optimized memory usage especially for synapse structures. Each currently uses only 12 bytes and stores the minimum amount of information needed for simulation.

### 3.1.3 The Visualizer

The third part of our BOSS system is the custom visualization software, Viz. It renders 3D models simulated by BOSS. Viz is written in C++ and can be compiled on different operating systems, including Microsoft Windows, Apple Mac OS X, and GNU/Linux. Viz depends on FLTK ("Fast Light Toolkit"), a cross-platform GUI toolkit written in C++ that supports OpenGL. Figure 31 illustrates the user interface of VIZ.

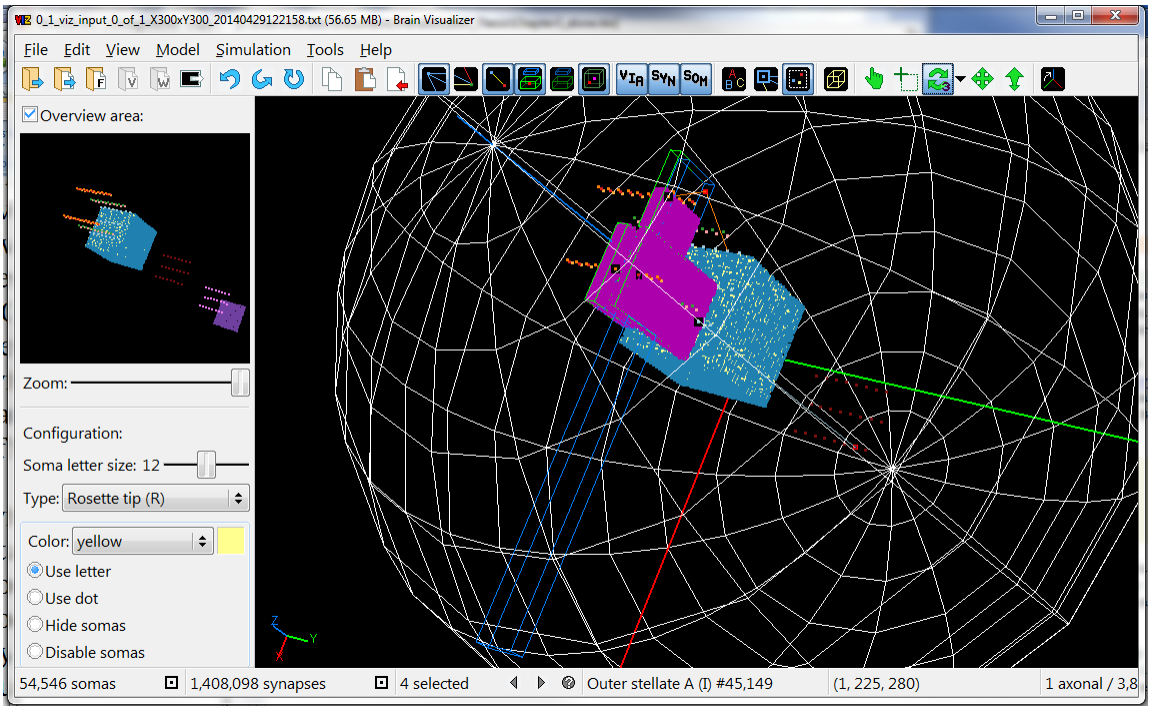


Figure 31: Illustration of the VIZ user interface.

Viz can render models with up to a billion synapses on a lab PC. It can display detailed static models of neuronal networks, optionally showing synaptic connections and neuritic fields. There are also display modes for dynamic simulation results including color-coded neuronal activity by firing frequencies, by cell internal

voltages, or by synapse weight changes. Many of the images shown in this chapter of the dissertation have been created using Viz. Viz has been an invaluable tool in helping us refine our large cerebellar models.

## 3.2 The Cerebellum

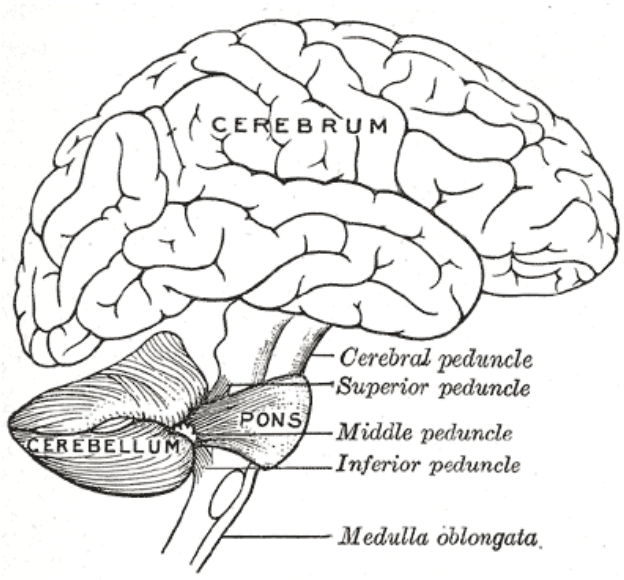


Figure 32: Illustration of the human brain including the cerebellum.

The cerebellum (Latin for "little brain") is a region of the brain that plays an important role in motor control. It may also be involved in some cognitive functions such as attention and language, and in regulating fear and pleasure responses; its movement-related functions are the most solidly established [74]. The cerebellum does not initiate movement, but it contributes to coordination, precision, and accurate timing of muscle contractions. It receives input from sensory systems of the spinal cord and from other parts of the brain, and integrates these inputs to fine tune

motor activity [25]. Cerebellar damage does not cause paralysis, but instead produces disorders in fine movement, equilibrium, posture, and motor learning [25]. Animals and humans with damaged or destroyed cerebella are still able to perform movements, but these movements will be slow, inexact, and poorly coordinated. Although the gross function of the cerebellum (motor control) is well known, there is no consensus on how it achieves coordination. Its regular structure, which has undergone much detailed neuroanatomical investigation, provides many hints.

The cerebellar cortex consists of three major and easily distinguishable layers: the outermost molecular layer, the ganglionic or Purkinje cell body layer, and the granular layer [22]. The molecular layer is built principally of dendritic arborizations and densely packed thin axons of granule cells, running parallel to the longitudinal axis of the folium, hence called parallel fibers. The cell bodies of only two types of neurons are localized in the molecular layer: the basket and the outer stellate cells. The dendritic ramifications of both neuron types are confined to the molecular layer, as are the axons of the outer stellate cells. The axon ramifications of the basket neurons are situated both in the molecular layer and the Purkinje cell layer, penetrating into the granular layer [22]. The Purkinje cell layer is a single sheet that contains the Purkinje cell bodies and several kinds of axons either ascending or descending between layers, as well as the ascending dendrites of Golgi cells. The granular layer is densely packed with billions of tiny granule neurons. A considerable portion of the granular layer space is occupied by the glomeruli, or rosettes, where mossy fibers synapse onto Golgi and granule cell dendrites [22,35]. Figure 33 shows the layers and some of the main cell types.

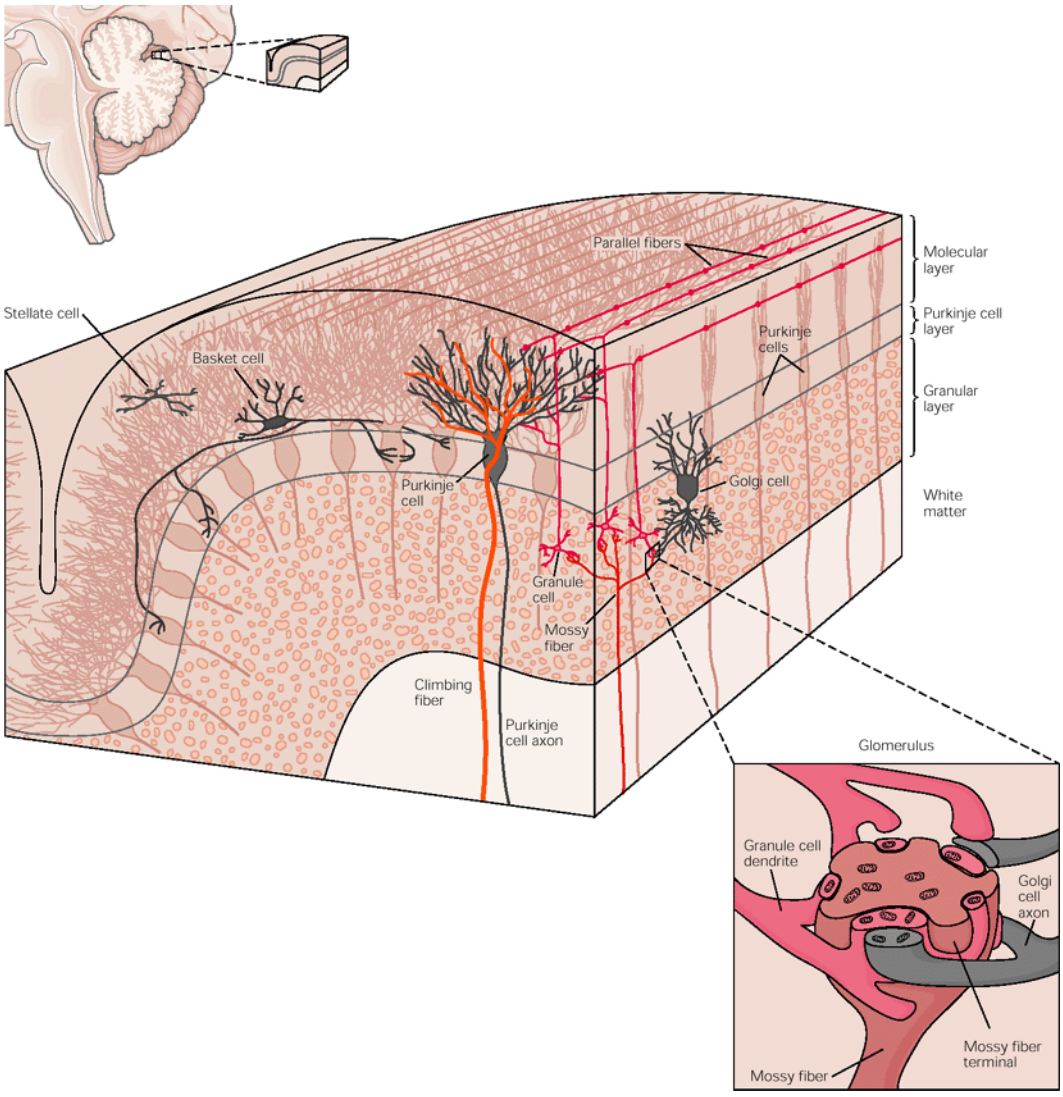


Figure 33: Illustration of cerebellum, its layers, and cell types. (Adapted from [35])

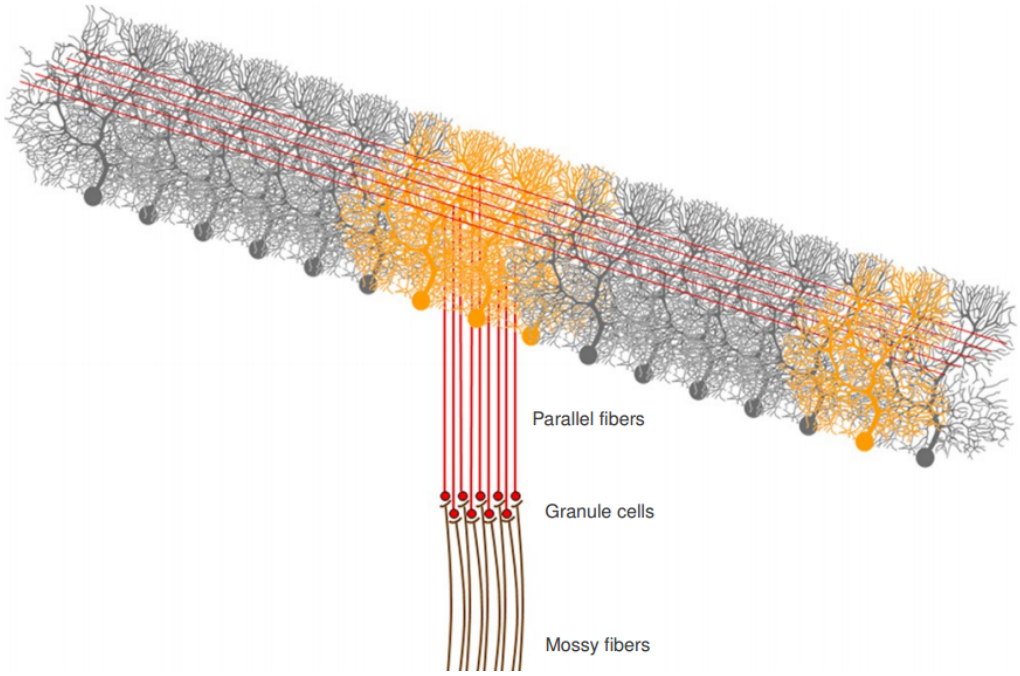


Figure 34: Illustration of a cerebellar "beam" consisting of parallel fibers and Purkinje cells. (Adapted from [35])

The cerebellum has five distinct well known neuron types: 1. Purkinje, the huge characteristic cell and the only output of the cerebellum, 2. granules, the most numerous neurons in the mammalian brain with characteristic long parallel fibers, plus inhibitory 3. basket, 4. stellate, and 5. Golgi cells. [22]. Inputs to the cerebellum come from two sets of axons: climbing and mossy fibers. The Purkinje cells are among the largest cells of the brain and each can form up to 200,000 input synapses each (in the human cerebellum). Granule cells are the most numerous cells in the brain. Their cell bodies are tiny but their long parallel fiber axons reach all the way to innervate the dendritic fields of Purkinje cells and give rise to the cerebellar "beams" as illustrated in Figure 34. Golgi cells receive inputs from mossy and parallel fibers, and inhibit the mossy fiber to granule cell synapses,

thus modulating the signal on the parallel fibers. Basket and stellate cells inhibit Purkinje cells. [22, 44–47]

Mossy fibers from various sources (pons, medulla, cerebrum) provide input to the granule cells, which in turn provide input to the Purkinje cells via the parallel fibers. Climbing fibers from the inferior olivary nucleus contact Purkinje cells directly. Each Purkinje cell receives excitatory input from just one climbing fiber. [22, 35].

## 3.3 Using BOSS to Create a Large-Scale Cerebellum Model

Given that the cerebellar cortex has the most regular anatomy of any brain region and that there is a wealth of structural information available, we decided that it would be possible to construct an accurate large-scale model of a big part of the cerebellum that could be used to test various theories on its function. The model has been a work in progress. We have gone through numerous iterations to improve its accuracy.

### 3.3.1 INIT Parameters for the Cerebellum

We used the extensive cerebellar literature, in particular the Sir John Eccles' book [22] and the Szentagothai series of publications [44–47], to gather detailed statistics about the cerebellum and tried to match as much as possible the cell shapes and densities in the three cerebellar layers and the synaptic connectivity.

```
$PARAMS
NCELLT = 12,
MSIMYMX = 6000, MSIMXMX = 2800,
$END
P N G B A S T I C M R D
P IS FOR PURKINJE CELLS
$CELL
MCY = 50, MCX = 75,
MAYY = 2, MAXX = 2, MAZZ = 2, MAZO =-10000,
DN = 2, MDY = 10,2, MDX = 240,2, MDZ = 320,2, MDZO = 160,-5,
...
SYNDA = 0,0,0,0,0,0,0,0,0,0,0,1000,
$END

N IS FOR GRANULE CELLS
$CELL
MCY = 5, MCX = 5, MCZLVL = -20, MCZ = -20, CZLN = 16,
MAYY = 3000, MAXX = 2, MAZZ = 2, MAZO = +0330,
MDY = 10, MDX = 10, MDZ = 20,
...
SYNDA = 1000,0,250,750,750,750,750,750,0,0,0,0,
$END
```

Figure 35: Sample parameters for cerebellar model

The input parameter file contains all the statistics for creating the structural model. Figure 35 shows an excerpt from a text file for a model of a 6,000 $\mu$m by 2,800 $\mu$m patch of cerebellar cortex. The model contains somas and synapses for 12 morphologically distinct types of neurons. Each thin (2x2 $\mu$m) granule cell axon, or "parallel fiber", extends 3,000 $\mu$m in the longitudinal (Y) direction [MAYY=3000]. Parameters are shown only for Purkinje cells plus their axonal and dendritic potential synapse regions and for the granule cells plus their synaptic regions. Electrical parameters for dendrites, somas, and axons have been elided

After one section ($PARAMS... \; END$) with overall model parameters, each input file has a section ($CELL... \; END$) dedicated to each cell type. The section for a cell type specifies the density and placement of its somas in the model space, the shapes and soma-relative positions of the axonal and dendritic synaptic regions for each soma, the density of synapses from its axons to each other cell type wherever their axonal and dendritic regions overlap, and electrical characteristics of its dendrites, somas, and axons.

The section for Purkinje (P) cells places the centers of all P-cell somas into a single plane at Z=0 (by default), at points 50 $\mu$m apart in Y (MCY) and 75 $\mu$m in X (MCX). The second line (MAYY) describes each P-cell's single tiny (2x2x2 $\mu$m) axonal region ending in the dentate nucleus 10,000 $\mu$m (MAZO) below the P-cell center. The third line (DN=2) gives the widths and locations of the two dendritic regions for each P-cell: the thin but huge (1i0x240x320 $\mu$m - MDY, MDX, MDZ) main dendritic tree above (MDZO=160 $\mu$m) each soma and a tiny (2x2x2 $\mu$m) synaptic region 5 $\mu$m ibelow (MDZO=-5) each soma center. P-cell electrical parameters for neurite signal propagation speeds, synapse strengths, and soma spiking behaviors are omitted. The last line (SYNDA) of synapse densities (in thousandths) reveals that each P-cell axon forms no (0) synapses except one (1000) where it overlaps ("touches") the dendritic region of a dentate nucleus cell (D), the

last type in the model.

Parameters in the section for granule cells (N) specify that granule centers are packed 5x5 $\mu$m apart below the P-cells in 16 (CZLN) layers 20 $\mu$m (MCZ) apart from Z=-20 $\mu$m (MCZLVL) to Z=-320$\mu$m. The next line (MAYY=3000) says that each tiny granule cell has a long, thin 2x3000x2 $\mu$m "parallel fiber" axon that extends 1,500 $\mu$m each way (+Y, -Y), passing through the dendritic trees of nearly 400 Purkinje cells. In this model, each granule cell interacts with afferent axon endings within its 10x10x20 $\mu$m dendritic synapse region. Each granule cell axon forms one synapse in all P-cell dendritic regions that it penetrates, in 25% of the Golgi cell regions, and in 75% each of the five types of inhibitory stellate interneurons found within the upper cortical (molecular) layer dominated by the densely packed dendritic trees of Purkinje cells.

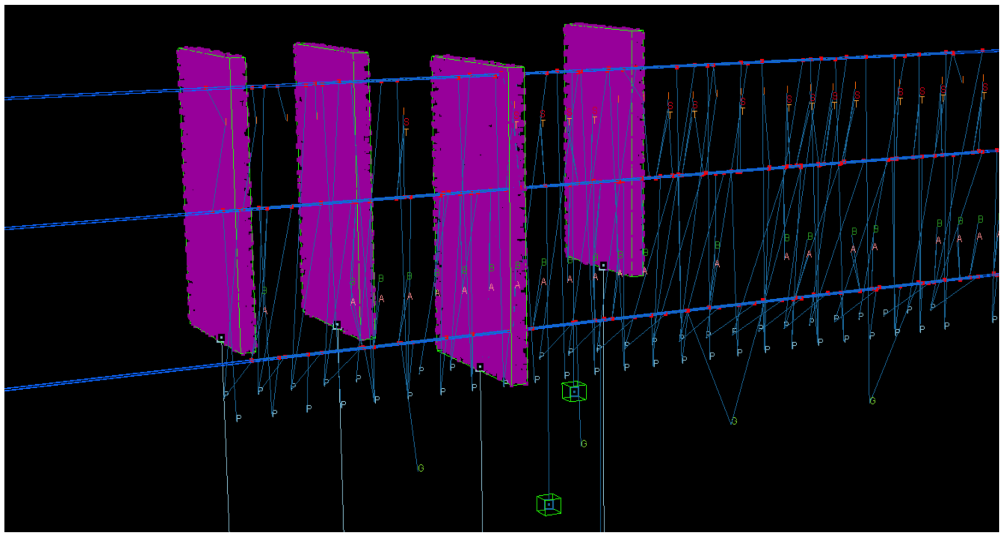

Figure 36: Four Purkinje and three granule cells visualized.

We use our visualization code to inspect and analyze models created with

BOSS. Figure 30 in the earlier section shows an image that represents a tiny section of a cerebellar model our application created when configured to generate the model shown by the parameter file that we explained above. The two horizontal lines at the top of the image are the two parallel fiber axons from the two granule cells. Each of these long axonal fibers passes through many hundreds of dendritic regions. In the sample model of four neurons, the overlapped regions were identified, and fifteen synapses were placed in accordance with the statistical parameters provided in the input configuration file. Figure 36 shows another tiny zoomed-in example of a model with four Purkinje cells and three granule cells selected. They make up part of one cerebellar "beam", like the one shown in Figure 34.

### 3.3.2 Synapses, Learning, and Gap Junctions

Chemical synapses are created between type pairs that are well known to have connections with each other. Those synapses are formed wherever there is overlap (during the INIT phase) between axonal and dendritic fields. Most of the synapses have a fixed weight (i.e., they do not get strengthened or weakened). The values of weights are based on cerebellar literature and by adapting the values to get reasonable firing frequencies from the Izhikevich neurons.

The most important synapses are the ones between granule and Purkinje cells. They are known to be the main learning synapses in the cerebellum. [17, 32]. The learning method used is based on STDP (Spike Timing Dependent Plasticity) rules [8, 64]. Figures 34 and 37 show the location of these learning synapses between the granule parallel fibers and the Purkinje dendritic fields.

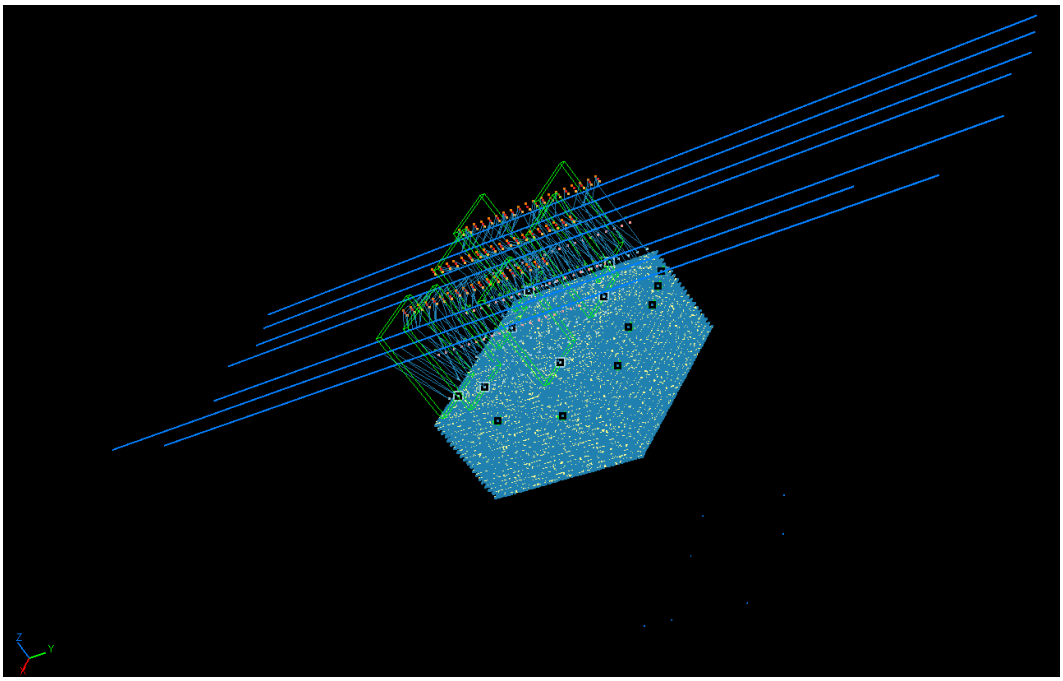

Figure 37: A small model of the cerebellum with some Purkinje cells and parallel fibers selected.

Non-chemical electrical synapses (or gap junctions) are also present in the cerebellum. See Section 2.3 for details on gap junctions. More specifically, there have been recent studies showing that neighboring Golgi cells form gap junctions with each other on their apical dendrites [18,70]. Gap junctions are created on those Golgi dendrites that overlap. Dendritic overlap detection is done by the same INIT code that finds overlaps during creation of chemical synapses.

### 3.3.3 Firing Activity of Cerebellar Cells

We are using the Izhikevich model for all neuron types in our simulations. As a first approximation for observed firing frequencies in our models, we chose the Regular Spiking Izhikevich parameters for the neuron types with low firing frequencies and

the Fast Spiking type for cell types with higher frequencies. The straight-forward dynamics of the Izhikevich model make it easy to modulate the firing frequencies of the cells to vary with the magnitude of total cell input.

We collected firing frequencies statistics of different cell types from cerebellar literature as shown in Table 4. We try to tune the Izhikevich neurons to have similar ranges of firing activity. In our simulations, we force fire different neurons to get firing activity started. Since the inputs to the cerebellum are the mossy fibers and the climbing fibers, we usually force fire those two cell types with frequencies that are comparable to biological recordings. We have implemented an image filter mechanism, where the pixel grayscale levels of an image are transformed into probabilities of force firing neuron types.

Table 4: Cerebellar cell firing frequencies by type

| Cell Type | Firing Frequency |
|---|---|
| Purkinje | 56.4 Hz (17-150 Hz) |
| Granule | 10-20 Hz |
| Golgi | 19.1 Hz |
| Basket | 33 Hz |
| Stellate | 33 Hz |
| Climbing Fiber | 1-2 Hz |
| Mossy Fiber | 50 Hz |
| Glomerulii | 50 Hz |

### 3.3.4 Examples of Our Cerebellar Models

We have developed a range of models of different sizes and firing parameters depending on the particular behavior that we are tuning. The sizes of the models also depend highly on which computer runs the simulation. We are always trying to increase the size and efficiency of the models that we generate.

#### 3.3.4.1 Cerebellar Model Sizes and Ratios

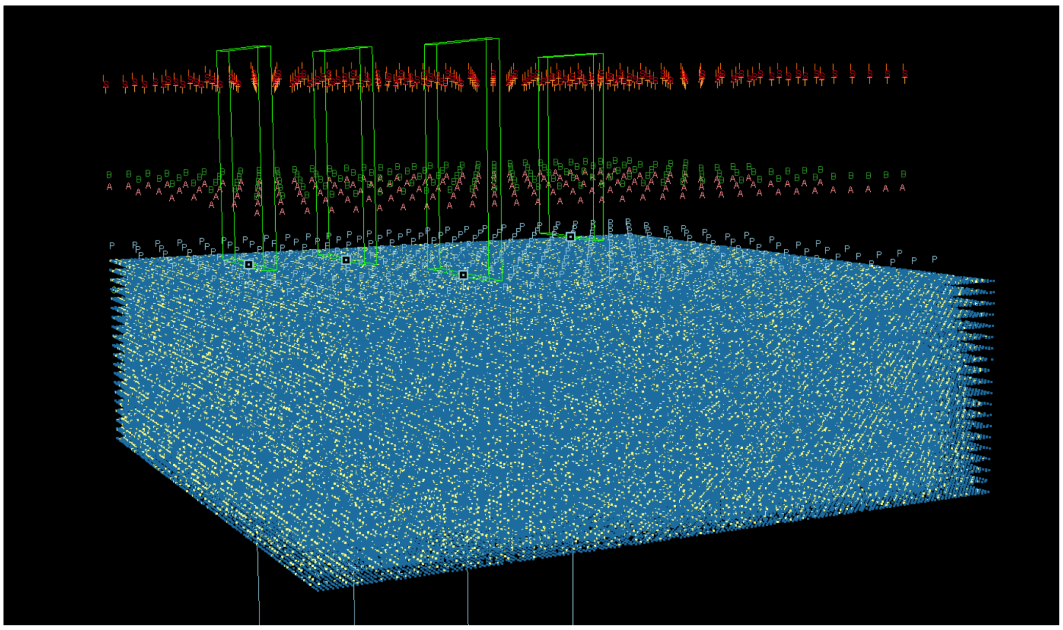

Figure 38: A 2.9 by 4.5 mm model of cat cerebellar cortex showing the tall dendritic regions of four Purkinje cells and the somas of 4,230 basket and 6,345 stellate cells above the plane of 3,437 Purkinje somas. The blue base has 6.5M (blue) granule somas and 1.3M (cream) mossy fiber rosettes.

Since the densities and sizes of cerebellar cell types differ drastically, the numbers of cells of each type are also quite different in our models. We always try to

match roughly the literature statistics on densities and count ratios.

Table 5: Cerebellar cell counts by type.

| Cell Type | Count (our model) 1400x1400 $\mu$m | Count (literature rough estimates) | Ratio per Purkinje (our model) | Ratio per Purkinje (literature) |
|---|---|---|---|---|
| Purkinje | 518 | 1.25 million | 1 | 1 |
| Granule | 985,242 | 2.2 billion | 1902 | 1769 |
| Golgi | 100 | 0.4 million | 0.19 | 0.33 |
| Basket | 616 | 7.3 million | 1.17 | 6 |
| Stellate | 924 | 20 million | 1.75 | 16 |
| Climbing Fiber | 518 | 1.25 million | 1 | 1 |
| Mossy Fiber | 4,900 | 5 million | 9.4 | 4 |
| Glomeruli | 195,950 | 80 million | 377 | 68 |
| Totals | 1,188,894 | 2.3 billion | - | - |

On a lab PC with 128 gigabytes (GBs) of memory, we have simulated electrical activity in networks with more than 20 million neurons and 4 billion synapses. On 1,024 NY-Blue nodes with a total of 2,048 GBs, we have run models of 700 million neurons connected by 125 billion synapses, roughly a fifth the size of the cat cerebellum. Table 5 shows the counts of the different cell types on a typical

small 1400 x 1400 $\mu$m patch of cerebellar tissue. A summary of some of the largest model sizes simulated on different platforms and with different amounts of RAM memory are presented in Table 6. We always target fast simulation performance and can get near real time simulations for tiny models of a few thousand neurons. Scaling and simulation runtimes depend highly on the hardware. For example, we can simulate 1 second of the large PC models (with 4 billion synapses) in less than 45 minutes, well within reasonable time frames.

Table 6: Large model sizes in different platforms

| Platform | Memory Size (GB) | Neuron Count | Synapse Count | Tissue Area ($mm^2$) |
|---|---|---|---|---|
| Real Time | Any | 5,600 | 1 million | 0.1 |
| Per 2GB | 2 | 600,000 | 125 million | 1 |
| PC Large | 128 | 22 million | 4 billion | 36 |
| Blue Gene/P | 1024x2 | 721 million | 126 billion | 1024 |

#### 3.3.4.2 Firing Activity in Two Examples

We ran numerous simulations to see the flow of firing activity from input (mossy fibers) to output (Purkinje cells). Firing activity of a sample model is illustrated in Figure 39 after we stimulated two beams of mossy fibers. Excitatory activity flowing from mossy fiber input reaches all the way to the Purkinje cells. A correct balance of excitation and inhibition is necessary for the model to display a reasonable amount of activity. The third panel (lower left) better illustrates the cerebellar

layers, with the large block of green dots showing millions of tiny granule cells.

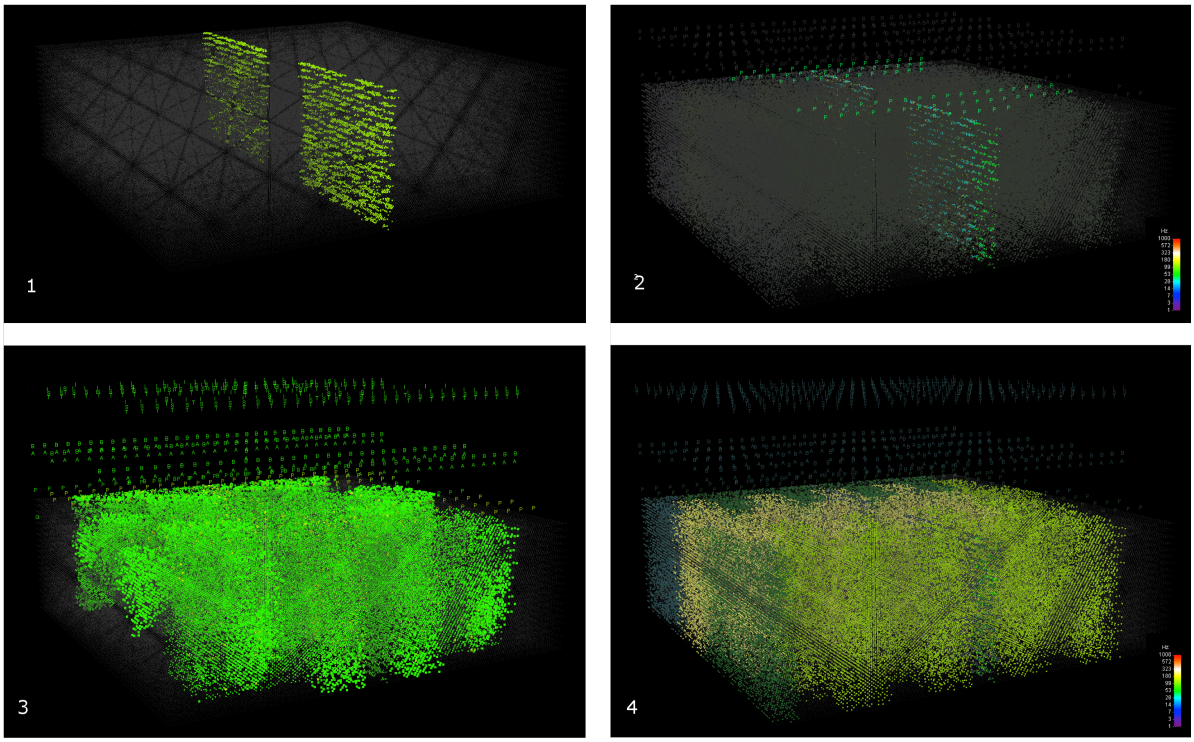


Figure 39: Firing rates of granule, Purkinje, stellate, and Golgi cells after activity in two wide beams of mossy fibers; the lower right color bars gauge firing rates from 1 (violet) to 1000 Hz (red).

We ran various simulations on another relatively small model with three circular patches of mossy fibers being force fired at a frequency of 66 Hz. As can be seen in the example simulation in Figure 40, the excitatory input travels up from the mossy fibers (panel 1), to the granule cells and the glomeruli rosettes (the cylinders in panel 2), and eventually excites the Purkinje cells (in panel 3). Panel 3 and 4 at the bottom show the spread of Golgi inhibition into the glomeruli (the rectangular dark purple flows around the cylinders). Some granule cells and Purkinje cells are selected to show the "cerebellar beams" along lines of parallel fibers.

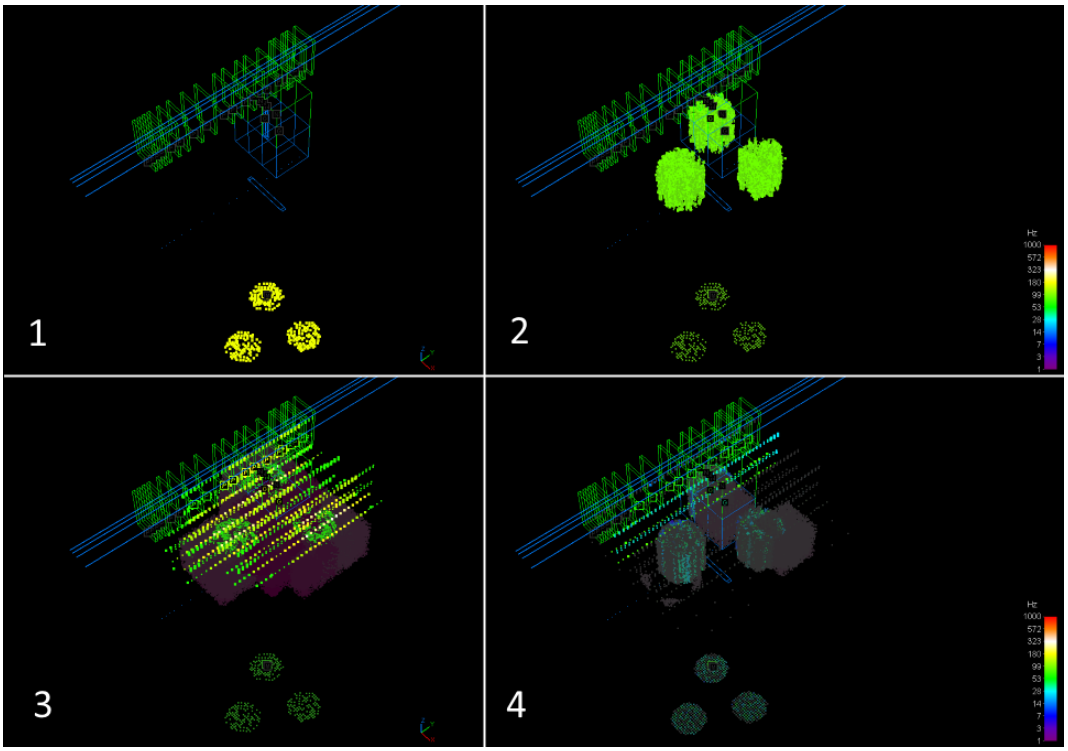


Figure 40: Firing activity on a 1.4x1.4mm small model

## 3.4 Golgi Cells, Their Inhibitory Effect on Cerebellar Activity, and the Role of Gap Junctions

One of the most important pathways of the cerebellum is the inhibitory loop resulting from Golgi cells' synaptic interactions. Golgi cells have a major role in the pathway of firing activity that travels from the Mossy Fibers to the granule cells (through the cell types illustrated in Figure 41).

As a crucial element in modulating overall cerebellar activity, the Golgi cells have been studied extensively. They are large inhibitory neurons that receive input from mossy and parallel fibers. They have a unique feature because they perform

their inhibitory function by forming a synapse on the mossy fiber to granule cell synapses themselves, thus modulating the excitatory synapse that goes through individual mossy fiber glomeruli (rosettes) to the granule cells.

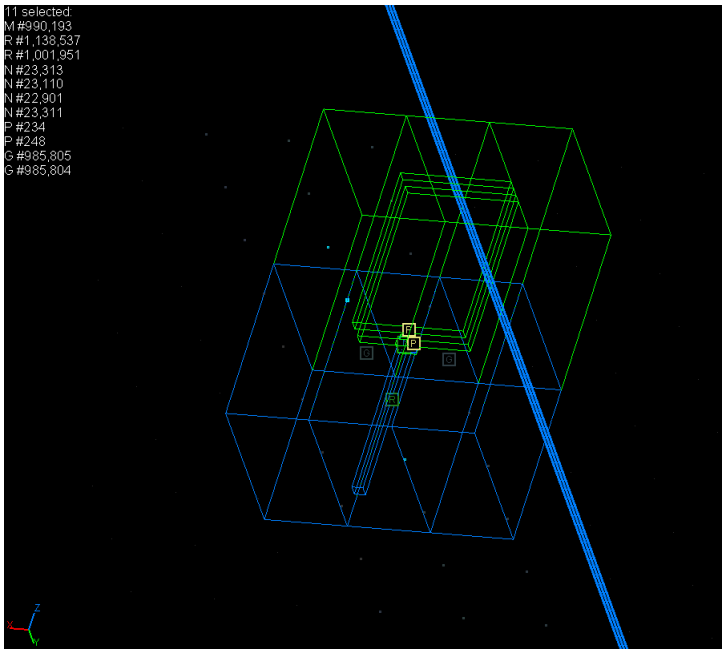


Figure 41: Neuritic fields of two Golgi cells, three granule parallel fibers, two Purkinjes, two rosettes, and one mossy fiber.

### 3.4.1 Golgi Anatomy

Even though it is known that Golgi cells play a crucial role in the cerebellar activity, there has been contradictory information in the iliterature about their exact anatomy and function. The density and potential overlap of Golgi cells have been debated. Sir John Eccles' book claims that Golgi cells do not overlap [22]. Many later studies have disagreed with that conclusion, since neuroanatomical experiments on different mammals have shown that the large Golgi neuritic fields have

some overlap [18, 47]. In recent years, it has been shown that Golgi cells not only overlap, but they also contain gap junctions in their apical dendrites [18, 70].

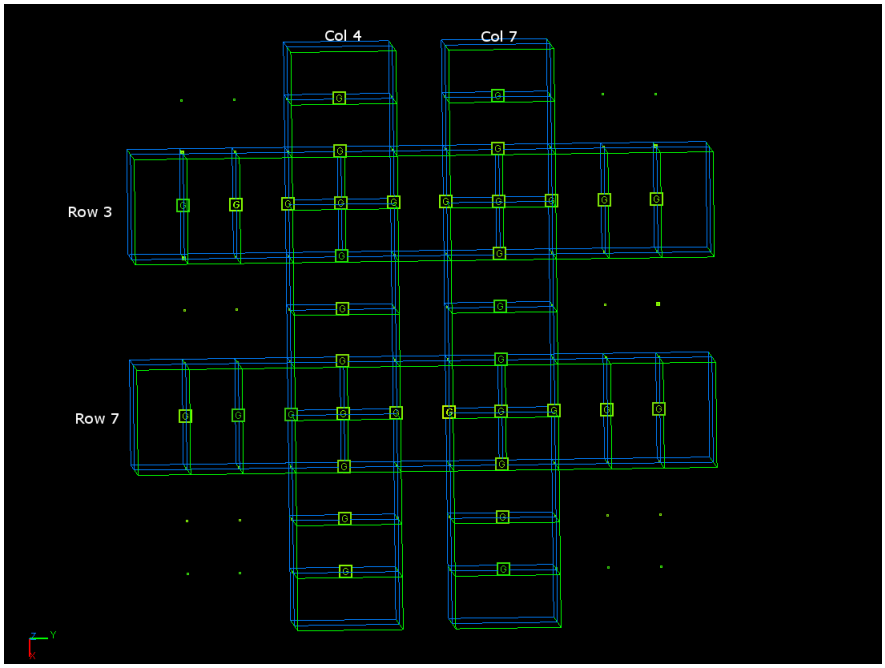


Figure 42: Top view of the Golgi cell layer with the selected cells showing the rows and columns for which we are analyzing synchrony.

For our implementation, we chose square Golgi neuritic fields of 300x300 $\mu$m. The Golgi cells were placed on the same layer, with their somas 150$\mu$m apart (as illustrated in Figures 41 and 42. Every Golgi neuritic field partially overlaps eight nearest neighbors with which it can form gap junctions. Each Golgi creates about 9,000 axonal connections to inhibit within the glomeruli rosettes, by blocking the amount of excitation that passes from each rosette to nearby granules. Each Golgi receives input from the mossy fibers via the same rosettes and, in its apical dendrites synapses with granular parallel fibers. Figure 41 shows three neighboring parallel

fibers (the almost vertical triplet of bright blue lines) piercing the large Golgi apical dendrites (the large green boxes). Figure 43 shows dozens of parallel fibers (horizontal blue lines) piercing the Golgi dendrites.

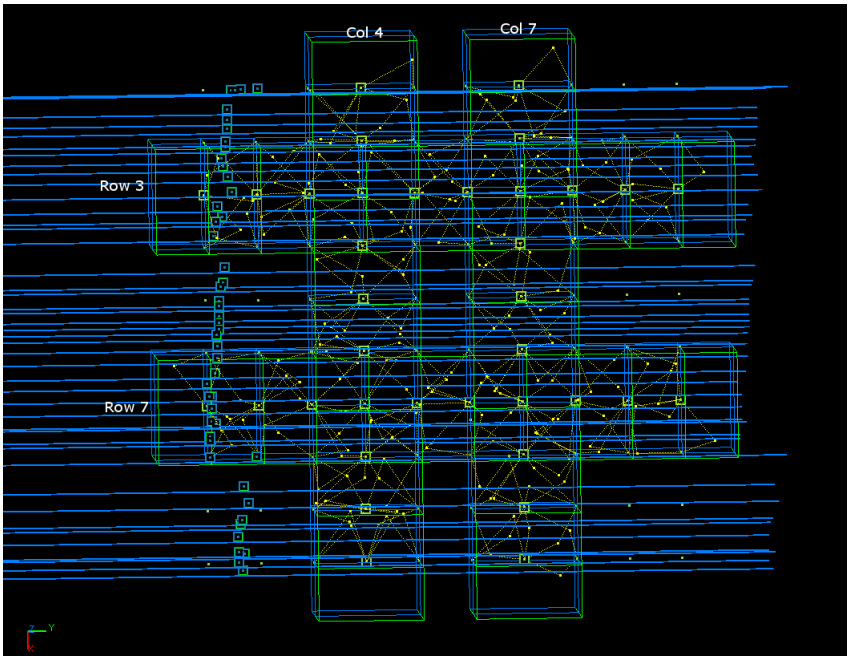


Figure 43: Top view of the Golgi cell layer with parallel fibers shown as blue lines running horizontally.

### 3.4.2 Synchrony of Golgi Cells

There have been a few studies looking at Golgi activity, in particular on how synchronized their firing is, and what influences that synchrony. For instance, Vos et. al. measured activity in pairs of Golgi cells in rats and concluded that Golgi cells that are in the same longitudinal axis (and thus receive common parallel fiber input) tend to be significantly more synchronized than the Golgi cells that are in the transverse axis [72]. Golgi cells that receive common parallel fiber inputs should fire

coherently, whereas Golgi cells without shared parallel fibers have less synchronized firing. We tested this theory using the 1400x1400 $\mu$m small version of our cerebellar model (subsection 3.3.4), which contains 100 Golgi cells in a 10x10 grid and a total of 1.2 million neurons, 83% granule cells. The structure of this model is the same as the one whose cell counts by type are in Table 5 as well as the firing images in Figure 40.

For our simulations, we randomly force fired at a high frequency of 200 Hz just 2% of the 4,900 mossy fibers in this model. Every 5 ms about 98 mossy fibers fire an action potential and send their excitatory signals upward to the glomeruli rosettes. This input style was chosen because it has no particular bias in terms of orientation or clustering since the mossy fiber cells are spread uniformly in one layer. The amount of excitation was chosen because it produces moderate firing activity overall in the model.

Since we are not limited by the same factors as laboratory scientists, we can record the voltages of entire longitudinal "rows" or transverse "columns" of Golgi cells and calculate their synchrony values without being limited to statistical analysis of electrode recordings from pairs of cells.

We selected a few Golgi cells and looked at their voltage traces and firing activity. Specifically, we selected two "rows" of ten Golgi cells each which are oriented longitudinally in the same direction as the parallel fibers, and two "columns" of ten Golgi cells each perpendicular (transversally) to the "rows". Figure 42 shows only the 10x10 grid of Golgi cells and the square dendritic fields for the forty selected cells; all other cells are hidden. Figure 43 shows the exact same model with many parallel fibers revealed to illustrate that the "Rows" represent Golgi cells aligned in the same direction as the parallel fibers.

The simulation ran for 1000 cycles (500 ms). We not only looked at some of the Golgi firing but also calculated the synchrony within each of the two rows and

two columns. Synchrony was calculated using the same Equation 9 in subsection 2.4.1 that measured the synchrony of Hypoglossal Motoneurons.

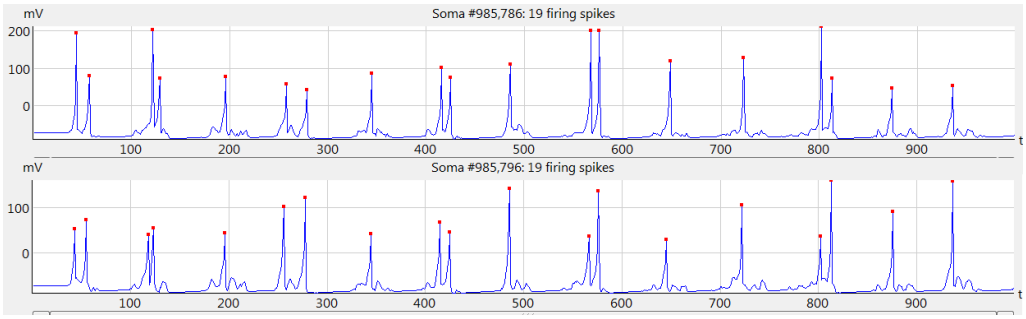


Figure 44: Voltage traces of two Golgi cells in one of the selected rows.

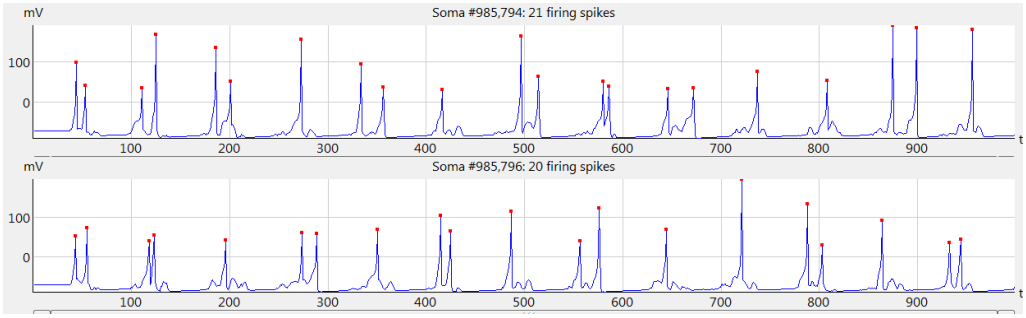


Figure 45: Voltage traces of two Golgi cells in one of the selected columns.

Figures 44 and 45 show pairs of voltage traces from two Golgi cells in the selected rows or columns to illustrate the firing pattern of Golgi cells in these simulations. The voltage traces of all ten Golgi cells in each row and column were used to calculate the synchrony values for each row and column in Figure 46. Subtle differences in the coherence of firing can be seen even in the raw voltage traces in Figure 44 and 45. The red dots on the voltage traces show times of Golgi cell firing spikes.

The results of our simulations (illustrated in the graph on Figure 46) confirm that Golgi cells in the same rows have significantly higher values of synchrony (0.494 for Row 3 and 0.483 for Row 7) than groups of Golgi cells oriented in columns (0.333 for Col 4 and 0.366 for Col 7). Our model is consistent in this particular feature with the experimental data of Vos et. al. [72].

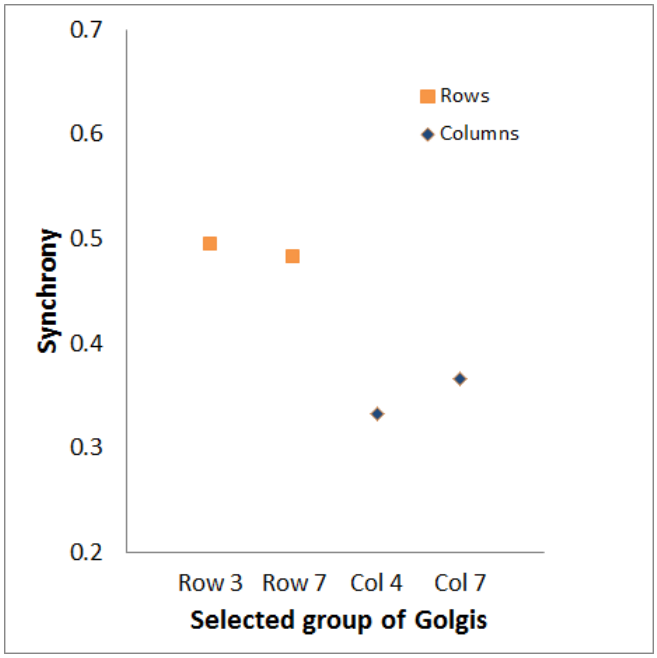


Figure 46: Synchrony levels of groups of Golgi cells.

We went a step further than the Vos study and analyzed whether strong gap junctions have an effect on the on-and off-row behavior. After having performed the original simulations with no gap junctions (Figures 44-46), we simulated the same model with gap junction conductances set to a reasonable value of 5 nS (nanoSiemens) and then to a very high value of 10 nS. As a preview of the synchrony results, we show the voltage traces for two Golgi cells from one of the rows and columns with the 5 nS gap junctions (Figures 47 and 48).

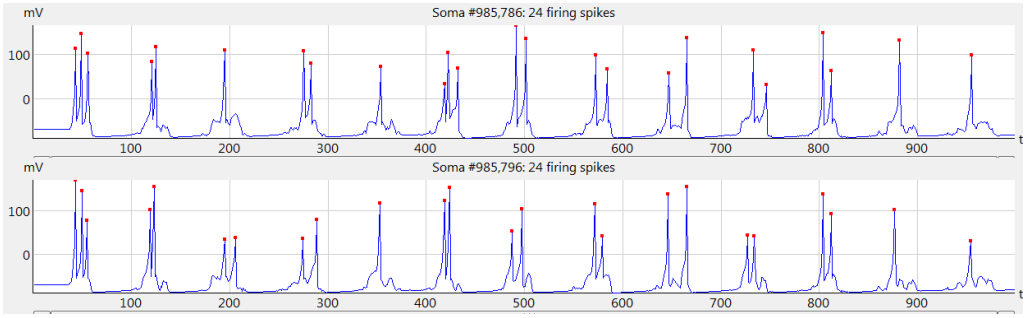


Figure 47: Voltage traces of two Golgi cells in one of the selected rows, with gap junctions at 5 nS.

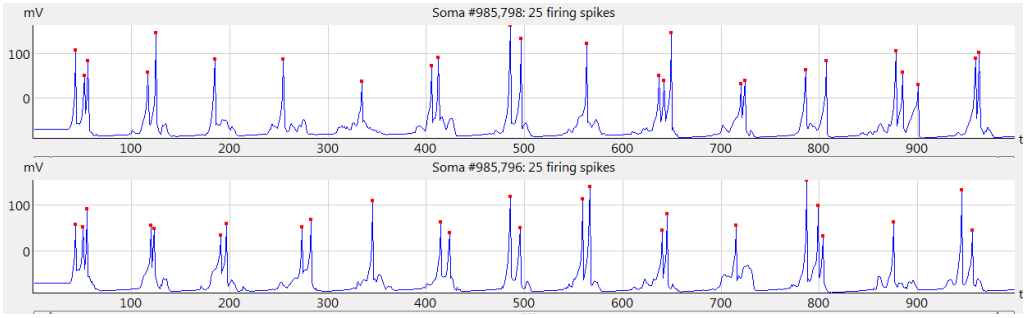


Figure 48: Voltage traces of two Golgi cells in one of the selected columns, with gap junctions at 5 nS.

The final results of the synchrony values show that gap junctions help synchronize the activity for all rows and columns. For high values of GJ conductance (10 nS), the disparity between levels of synchrony for rows and columns is lessened since all rows and columns reach a synchrony above 0.6. As mentioned in the HM Chapter 2 (Section 2.5), usually gap junctions cause an increase in synchrony levels. Depolarization or action potentials in one cell can cause depolarization or even increased firing in neighboring cells which leads to a higher degree of synchrony. As shown in Table 7 and in Figure 49, our GJ-connected Golgi cells consistently

demonstrate higher synchrony for higher conductance values as well as greater synchrony along parallel fiber bundles (rows) than across them (columns).

Table 7: Synchrony of Golgi cells

| Group \ GJ Conductance (nS) | 0 | 5 | 10 |
|---|---|---|---|
| Row 3 | 0.494 | 0.581 | 0.628 |
| Row 7 | 0.483 | 0.573 | 0.655 |
| Col 4 | 0.333 | 0.483 | 0.621 |
| Col 7 | 0.366 | 0.451 | 0.612 |

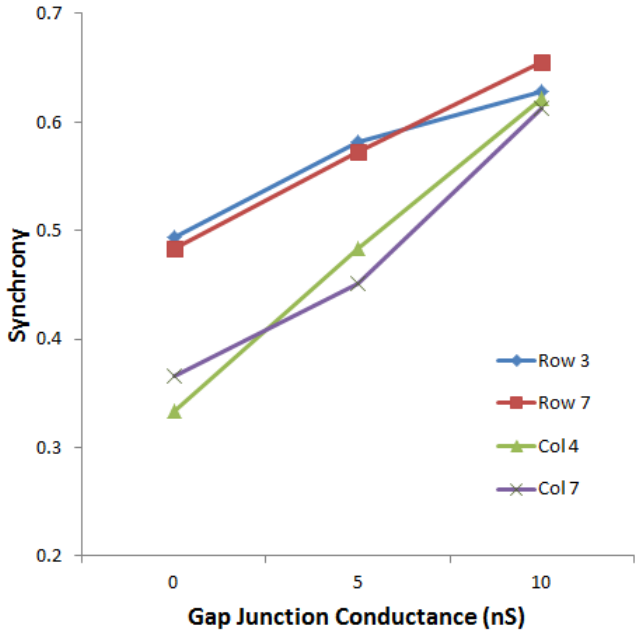


Figure 49: Synchrony levels of two rows and two columns of Golgi cells for different levels of gap junction conductance. Data are same as in Table 7.

### 3.4.3 Importance of Golgi Inhibition and Its Effect on Purkinje Firing Frequency

The simulations in the previous section illustrate other important Golgi features, the inhibitory effect of the Golgi cells even on their own firing activity and on the overall granular layer. Even though they are getting excitatory input of high frequency (200 Hz), they do not produce action potentials with the same frequency, and they do not reach perfect synchrony but are only moderately coherent. The Golgi cells on the same row had a synchrony value of 0.48-0.49 out of 1.00 without gap junctions and still only 0.63-0.65 with extremely strong (10 nS) gap junctions. That Golgi cells show only moderate synchrony and limited firing rates has been reported in studies of Golgi firing activity [18]. The moderate firing can be attributed to the inhibitory loop by which Golgi cells when they fire, block the excitation passing from the mossy fibers to the granule cells, in turn lowering the input that the Golgi cells receive from parallel fibers.

The only "output" cells from the cerebellum and the most iconic cerebellar cell is the Purkinje. As such, it is important to use simulations to analyze different factors that influence the firing activity of Purkinje cells. It is well known that Golgi cells play a significant role in the firing activity of the granular layer [18] via the inhibitory mechanisms on the glomeruli, described in Section 3.2. Since the granular parallel fibers are the main input to Purkinje cells, we expect that Golgi cell inhibition plays a crucial role in modulating Purkinje firing frequency. Our implementation of Golgi inhibition involves a fraction of pre-synaptic suppression (e.g., 1/4 means only 1/4 of any firing spike excitation passes from a mossy fiber to granule dendrites in the synaptic complex within a glomerulus). The half-life of suppression is usually set at 5 ms. In the first 5 ms, immediately after a Golgi cell fires, all mossy-granule cell synapses that are part of each glomerulus connected

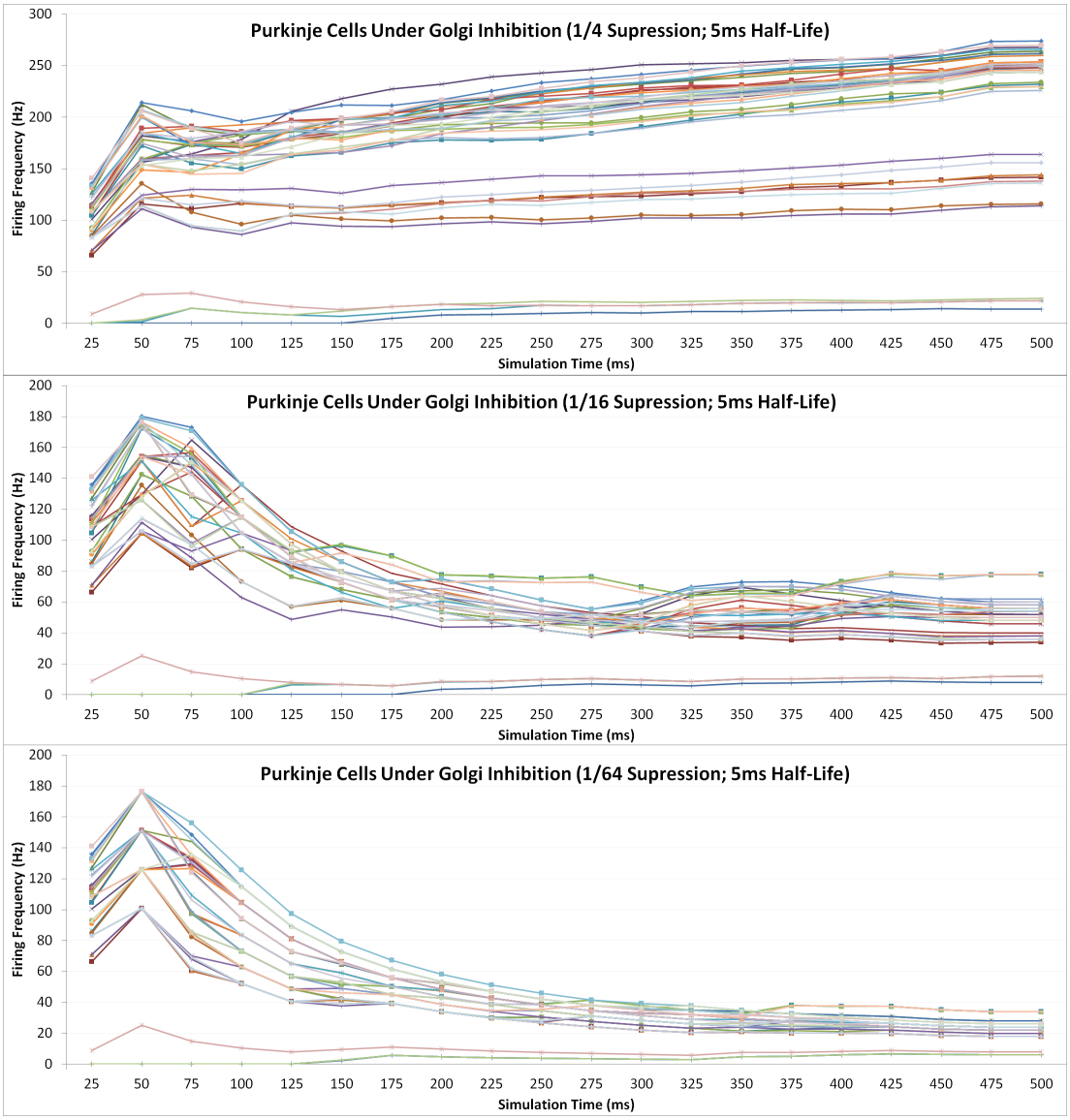


Figure 50: Firing frequencies of Purkinje cells for three values of Golgi inhibition

to the Golgi will only transmit one fourth of the excitation, then one half of the excitation in the next 5 ms, and inhibition will be inactive after that period until the Golgi fires next.

We tested the effects of inhibition by running simulations with different duration of strong suppression. The excitatory input provided to the system was a fairly strong pattern of firing from mossy fibers at 66 Hz with three spots set at the vertices of an equilateral triangle. A simulation with a similar forced firing stimulus drive was shown in Figure 40. The three levels of Golgi inhibition chosen were starting allowing excitation transmission fractions of 1/4, 1/16 and 1/64. All fractions have the same half-life of 5 ms, making the duration of significant inhibition for the first one only 10 ms, but 30 ms for the last one.

We selected 40 Purkinje cells and measured their firing frequency for a 500 ms simulation with 25 ms time bins. Figure 50 shows the firing frequencies of the Purkinje cells for three separate simulations where the only difference was their Golgi inhibitory strength. The pattern of modulation of Purkinje firing frequency is very clear. For the first simulation, the Golgi inhibition is not strong enough (1/4 excitation transmission) and does not last long enough, which causes the Purkinje cells to fire often and to reach unrealistically high firing frequencies of more than 200 Hz. When the suppression is set to 1/16, the firing frequency of most of the Purkinje cells settles within a stable range of 40-65 Hz, which is a quite reasonable firing rate for Purkinje cells in vivo. For suppression set at 1/64 (fraction of excitation transmission), the initial inhibition is too strong and its duration too long; the firing frequency keeps dropping in the simulation and reached below 40 Hz for all Purkinje cells.

The effect of Golgi suppression on Purkinje cells firing rate is also nicely illustrated by picking one Purkinje cell and looking at the voltage trace of the same cell (Figure 51) for each of the three simulations used to produce Figure 50. The

number of Purkinje cell firing spikes during 1000 cycles simulating 500 ms of network activity varies from 125 spikes with only 1/4 initial passing of mossy fiber excitation to granule cells, to 69 spikes at an initial 1/16 level, and to only 58 Purkinje spikes at an initial 1/64 passing of excitation from mossy fibers to granule cells thence to Purkinje cells.

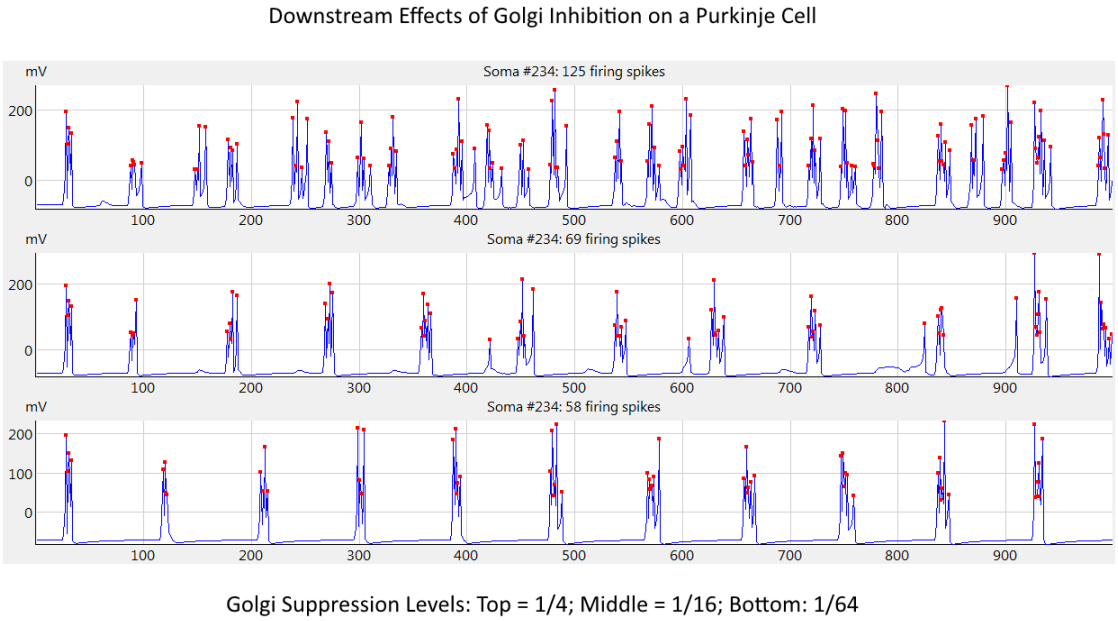


Figure 51: Voltage traces of a Purkinje cell

These simulations and the analysis of Purkinje firing frequencies again confirmed expectations on behaviors of the cerebellar circuitry. In this case, we showed the importance of Golgi cells on the overall activity of the cerebellum and in particular, how stronger Golgi inhibition reduces the firing frequency of Purkinje cells.

# Chapter 4

# Concluding Remarks

Computational neuroscience can be a very influential research area in providing better tools and approaches to understand the brain. In this dissertation, we presented two computational modeling projects of networks of neurons. The projects were different on many levels: the brain systems that we were studying, the type of biological detail of the models, the network size and computational requirements, and many other aspects. They are, however, both part of a similar approach and type of analysis that is commonly used in modern computational neuroscience. We created models of networks of neurons that attempt to replicate the activity of their biological counterparts. The models of individual neurons consist of differential equations that control the state of each neuron and the generation of its action potentials. Parameters specify individual neuron details and the connectivity of the networks. All simulations follow a similar pattern. After the model is generated, an external input is supplied, and numerical integration updates the state of each neuron at every time step. We record the state of some of the neurons, and we also analyze the networks as a whole by calculating average firing frequencies or synchrony.

The first project involved a lot of single-neuron biophysical details. Its main goal was to shed light on the factors that influence the synchronized behavior of

a small network of motoneurons. Our models were successful in providing insights and allowing detailed analysis of factors that can affect network synchrony including studies of gap junction blockade and changes in firing frequency (after input current amplitude changes and alterations to specific ion channels that affect excitability). The numerous simulations led us to observations that were even unexpected at first, such as the spontaneous CPG-like behavior.

The second project, BOSS, had a somewhat different focus. It involved years of coding to build a complete simulation software system for large-scale brain models. When creating large network models, the focus is more on aspects like general morphology and connectivity of the systems and less on single cell electrophysiology. For the scope of this dissertation, we targeted the cerebellum as a well-documented brain structure, and dove deeply into reproducing its overall structure. Considering the size of the models that we simulated (hundreds of millions of neurons and hundreds of billions of synapses), BOSS reached its goal of modeling huge numbers of neurons in structured networks. In addition, our models have taught us important details about specific features of the cerebellar functionality.

The two projects share even some of the behavioral analyses of the two networks. Gap junctions were simulated similarly in the network of HMs and between Golgi cells in the large cerebellar models. Even though synchrony analysis was the main focus of the first project, it was also used for one of our studies in cerebellar models. The numerous simulations that were performed have provided the evidence for the findings that are presented in this dissertation.

# Bibliography

[1] V. Alvarez-Maubecin, F. Garcia-Hernandez, J. Williams, and E. Van Bockstaele. Functional coupling between neurons and glia. *The Journal of Neuroscience*, 20(11):4091–4098, 2000.

[2] R. Ananthanarayanan, S. K. Esser, H. D. Simon, and D. S. Modha. The cat is out of the bag: cortical simulations with $10^9$ neurons, $10^{13}$ synapses. In *High Performance Computing Networking, Storage and Analysis, Proceedings of the Conference*, pages 1–12. IEEE, 2009.

[3] R. Ananthanarayanan and D. S. Modha. Anatomy of a cortical simulator. In *Proceedings of the 2007 ACM/IEEE Conference on Supercomputing*, page 3. ACM, 2007.

[4] E. Bailey and R. Fregosi. Coordination of intrinsic and extrinsic tongue muscles during spontaneous breathing in the rat. *Journal of Applied Physiology*, 96(2):440–449, 2004.

[5] D. Belliveau and C. Naus. Cellular localization of gap junction mrnas in developing rat brain (part 2 of 2). *Developmental Neuroscience*, 17(2):90–96, 1995.

[6] N. Belluardo, M. G., A. Trovato-Salinaro, S. Le Gurun, A. Charollais, V. Serre-Beinier, G. Amato, P. Meda, and D. Condorelli. Expression of connexin36 in the adult and developing rat brain1. *Brain Research*, 865(1):121–138, 2000.

[7] M. Bennett and R. Zukin. Electrical coupling and neuronal synchronization in the mammalian brain. *Neuron*, 41(4):495–511, 2004.

[8] G. Bi and M. Poo. Synaptic modification by correlated activity: Hebb's postulate revisited. *Annual Review of Neuroscience*, 24(1):139–166, 2001.

[9] C. Bou-Flores and A. Berger. Gap junctions and inhibitory synapses modulate inspiratory motoneuron synchronization. *Journal of Neurophysiology*, 85(4):1543–1551, 2001.

[10] R. Brette, M. Rudolph, T. Carnevale, M. Hines, D. Beeman, J. M. Bower, M. Diesmann, A. Morrison, P. H. Goodman, F. C. Harris Jr, et al. Simulation of networks of spiking neurons: a review of tools and strategies. *Journal of Computational Neuroscience*, 23(3):349–398, 2007.

[11] T. G. Brown. On the nature of the fundamental activity of the nervous centres; together with an analysis of the conditioning of rhythmic activity in progression, and a theory of the evolution of function in the nervous system. *The Journal of Physiology*, 48(1):18–46, 1914.

[12] R. Bruzzone and C. Ressot. Connexins, gap junctions and cell-cell signalling in the nervous system. *European Journal of Neuroscience*, 9(1):1–6, 1997.

[13] R. L. Calabrese. Half-center oscillators underlying rhythmic movements. *Nature*, 261:146–148, 1995.

[14] D. L. Cardone, T. J. Halat, M. N. Rodriguez, and I. C. Solomon. Expression of gap junction proteins in cranial (hypoglossal) and spinal (phrenic) respiratory motor nuclei in rat. *FASEB J*, 16:A810, 2002.

[15] C. Chow and N. Kopell. Dynamics of spiking neurons with electrical coupling. *Neural Computation*, 12(7):1643–1678, 2000.

[16] B. W. Connors and M. A. Long. Electrical synapses in the mammalian brain. *Annu. Rev. Neurosci.*, 27:393–418, 2004.

[17] E. D'Angelo and C. I. De Zeeuw. Timing and plasticity in the cerebellum: focus on the granular layer. *Trends in Neurosciences*, 32(1):30–40, 2009.

[18] E. D'Angelo, S. Solinas, J. Mapelli, D. Gandolfi, L. Mapelli, and F. Prestori. The cerebellar golgi cell and spatiotemporal organization of granular layer activity. *Frontiers in Neural Circuits*, 7, 2013.

[19] J. B. Dean, D. Ballantyne, D. L. Cardone, J. S. Erlichman, and I. C. Solomon. Role of gap junctions in $co_2$-chemoreception and respiratory control. *Respiration Physiology*, 129(1-2):83–100, 2001.

[20] R. Dermietzel and D. Spray. Gap junctions in the brain: where, what type, how many and why? *Trends in Neurosciences*, 16(5):186–192, 1993.

[21] M. J. Dizon and K. Khodakhah. The role of interneurons in shaping purkinje cell responses in the cerebellar cortex. *The Journal of Neuroscience*, 31(29):10463–10473, 2011.

[22] J. Eccles, M. Itō, and J. Szentágothai. *The cerebellum as a neuronal machine*. Springer-Verlag, 1967.

[23] C. Eliasmith, T. C. Stewart, X. Choo, T. Bekolay, T. DeWolf, Y. Tang, and D. Rasmussen. A large-scale model of the functioning brain. *Science*, 338(6111):1202–1205, 2012.

[24] J. Feldman and D. McCrimmon. Neural control of breathing. *Fundamental Neuroscience,*, 2003.

[25] E. J. Fine, C. C. Ionita, and L. Lohr. The history of the development of the cerebellar examination. In *Seminars in Neurology*, volume 22, pages 375–384. Thieme Medical Publishers, Inc., 2002.

[26] P. Gleeson, S. Crook, R. C. Cannon, M. L. Hines, G. O. Billings, M. Farinella, T. M. Morse, A. P. Davison, S. Ray, U. S. Bhalla, et al. Neuroml: a language for describing data driven models of neurons and networks with a high degree of biological detail. *PLoS Computational Biology*, 6(6):e1000815, 2010.

[27] W. Gropp, E. Lusk, N. Doss, and A. Skjellum. A high-performance, portable implementation of the mpi message passing interface standard. *Parallel Computing*, 22(6):789–828, 1996.

[28] D. Hansel, G. Mato, C. Meunier, and L. Neltner. On numerical simulations of integrate-and-fire neural networks. *Neural Computation*, 10(2):467–483, 1998.

[29] M. Helias, S. Kunkel, G. Masumoto, J. Igarashi, J. M. Eppler, S. Ishii, T. Fukai, A. Morrison, M. Diesmann, et al. Supercomputers ready for use as discovery machines for neuroscience. *Frontiers in Neuroinformatics*, 6:26–26, 2011.

[30] A. Hodgkin and A. Huxley. The components of membrane conductance in the giant axon of loligo. *The Journal of Physiology*, 116(4):473–496, 1952.

[31] K. G. Horn, H. Memelli, and I. C. Solomon. Emergent central pattern generator behavior in gap junction-coupled hodgkin-huxley style neuron model. *Computational Intelligence and Neuroscience*, 2012:10, 2012.

[32] P. Isope and B. Barbour. Properties of unitary granule cell to purkinje cell synapses in adult rat cerebellar slices. *The Journal of Neuroscience*, 22(22):9668–9678, 2002.

[33] E. M. Izhikevich and G. M. Edelman. Large-scale model of mammalian thalamocortical systems. *Proceedings of the National Academy of Sciences*, 105(9):3593–3598, 2008.

[34] E. M. Izhikevich et al. Simple model of spiking neurons. *IEEE Transactions on Neural Networks*, 14(6):1569–1572, 2003.

[35] E. R. Kandel, J. H. Schwartz, T. M. Jessell, et al. *Principles of Neural Science*, volume 4. McGraw-Hill New York, 2000.

[36] O. Kiehn and M. C. Tresch. Gap junctions and motor behavior. *Trends in Neurosciences*, 25(2):108–115, 2002.

[37] J. Kozloski and J. Wagner. An ultrascalable solution to large-scale neural tissue simulation. *Frontiers in Neuroinformatics*, 5:15, 2011.

[38] E. Marder and D. Bucher. Central pattern generators and the control of rhythmic movements. *Current Biology*, 11(23):R986–R996, 2001.

[39] H. Markram. The blue brain project. *Nature Reviews Neuroscience*, 7(2):153–160, 2006.

[40] D. A. McCrea and I. A. Rybak. Modeling the mammalian locomotor cpg: insights from mistakes and perturbations. *Progress in Brain Research*, 165:235–253, 2007.

[41] H. Memelli, K. G. Horn, L. D. Wittie, and I. C. Solomon. Analyzing the effects of gap junction blockade on neural synchrony via a motoneuron network computational model. *Computational Intelligence and Neuroscience*, 2012:8, 2012.

[42] K. Moortgat, T. Bullock, and T. Sejnowski. Gap junction effects on precision and frequency of a model pacemaker network. *Journal of neurophysiology*, 83(2):984–997, 2000.

[43] P. Pakhotin and A. Verkhratsky. Electrical synapses between bergmann glial cells and purkinje neurones in rat cerebellar slices. *Molecular and Cellular Neuroscience*, 28(1):79–84, 2005.

[44] M. Palkovits, P. Magyar, et al. Quantitative histological analysis of the cerebellar cortex in the cat. iii. structural organization of the molecular layer. *Brain Research*, 34(1):1–18, 1971.

[45] M. Palkovits, P. Magyar, et al. Quantitative histological analysis of the cerebellar cortex in the cat. iv. mossy fiber-purkinje cell numerical transfer. *Brain Research*, 45(1):15–29, 1972.

[46] M. Palkovits, P. Magyar, and J. Szentagothai. Quantitative histological analysis of the cerebellar cortex in the cat: i. number and arrangement in space of the purkinje cells. *Brain Research*, 32(1):1–13, 1971.

[47] M. Palkovits, P. Magyar, and J. Szentagothai. Quantitative histological analysis of the cerebellar cortex in the cat: ii. cell numbers and densities in the granular layer. *Brain Research*, 32(1):15–30, 1971.

[48] J. Peever and J. Duffin. Bilateral synchronisation of respiratory motor output in rats: adult versus neonatal in vitro preparations. *Pflugers Archiv European Journal of Physiology*, 442(6):943–951, 2001.

[49] J. L. Perez-Velazquez and P. L. Carlen. Gap junctions, synchrony and seizures. *Trends in Neurosciences*, 23(2):68–74, 2000.

[50] B. Pfeuty, G. Mato, D. Golomb, and D. Hansel. Electrical synapses and synchrony: the role of intrinsic currents. *The Journal of Neuroscience*, 23(15):6280, 2003.

[51] D. Purves, D. Fitzpatrick, L. Katz, A. Lamantia, J. McNamara, S. Williams, and G. Augustine. *Neuroscience*. Sinauer Associates, Incorporated, 2012.

[52] L. K. Purvis and R. J. Butera. Ionic current model of a hypoglossal motoneuron. *Journal of Neurophysiology*, 93(2):723–733, 2005.

[53] J. Rekling, G. Funk, D. Bayliss, X. Dong, and J. Feldman. Synaptic control of motoneuronal excitability. *Physiological reviews*, 80(2):767–852, 2000.

[54] R. Rozental, M. Srinivas, and D. C. Spray. How to close a gap junction channel. *Methods in Molecular Biology*, 154:447–476, 2001.

[55] A. A. Sharp, F. K. Skinner, and E. Marder. Mechanisms of oscillation in dynamic clamp constructed two-cell half-center circuits. *Journal of Neurophysiology*, 76(2):867–883, 1996.

[56] A. Sherman and J. Rinzel. Model for synchronization of pancreatic beta-cells by gap junction coupling. *Biophysical journal*, 59(3):547–559, 1991.

[57] A. Sherman and J. Rinzel. Rhythmogenic effects of weak electrotonic coupling in neuronal models. *Proceedings of the National Academy of Sciences*, 89(6):2471, 1992.

[58] J. C. Smith, A. Abdala, H. Koizumi, I. A. Rybak, and J. F. Paton. Spatial and functional architecture of the mammalian brain stem respiratory network: a hierarchy of three oscillatory mechanisms. *Journal of Neurophysiology*, 98(6):3370–3387, 2007.

[59] I. C. Solomon. Connexin36 distribution in putative $co_2$ chemosensitive brainstem regions in rat. *Respiratory Physiology and Neurobiology*, 139(1):1–20, 2003.

[60] I. C. Solomon, K. H. Chon, and M. Rodriguez. Blockade of brain stem gap junctions increases phrenic burst frequency and reduces phrenic burst synchronization in adult rat. *Journal of neurophysiology*, 89(1):135–149, 2003.

[61] I. C. Solomon and J. B. Dean. Gap junctions in $co_2$-chemoreception and respiratory control. *Respiratory Physiology and Neurobiology*, 131(3):155–173, 2002.

[62] I. C. Solomon, T. J. Halat, M. R. El-Maghrabi, and M. H. O'Neal III. Localization of connexin26 and connexin32 in putative $co_2$-chemosensitive brainstem regions in rat. *Respiration Physiology*, 129(1-2):101–121, 2001.

[63] I. C. Solomon, T. J. Halat, R. El Maghrabi, and M. H. O'Neal III. Differential expression of connexin26 and connexin32 in the pre-botzinger complex of

neonatal and adult rat. *The Journal of Comparative Neurology*, 440(1):12–19, 2001.

[64] S. Song, K. D. Miller, and L. F. Abbott. Competitive hebbian learning through spike-timing-dependent synaptic plasticity. *Nature Neuroscience*, 3(9):919–926, 2000.

[65] W. St John, J. Paton, and J. Leiter. Uncoupling of rhythmic hypoglossal from phrenic activity in the rat. *Experimental Physiology*, 89(6):727–737, 2004.

[66] J. Szabadics, A. Lorincz, and G. Tamais. Beta and gamma frequency synchronization by dendritic gabaergic synapses and gap junctions in a network of cortical interneurons. *The Journal of Neuroscience*, 21(15):5824–5831, 2001.

[67] G. Tamás, E. H. Buhl, A. Lörincz, and P. Somogyi. Proximally targeted gabaergic synapses and gap junctions synchronize cortical interneurons. *Nature Neuroscience*, 3(4):366–371, 2000.

[68] R. Traub, N. Kopell, A. Bibbig, E. Buhl, F. LeBeau, and M. Whittington. Gap junctions between interneuron dendrites can enhance synchrony of gamma oscillations in distributed networks. *The Journal of Neuroscience*, 21(23):9478–9486, 2001.

[69] C. Vergara, R. Latorre, N. Marrion, and J. Adelman. Calcium-activated potassium channels. *Current Opinion in Neurobiology*, 8(3):321–329, 1998.

[70] K. Vervaeke, A. Lőrincz, P. Gleeson, M. Farinella, Z. Nusser, and R. A. Silver. Rapid desynchronization of an electrically coupled interneuron network with sparse excitatory synaptic input. *Neuron*, 67(3):435–451, 2010.

[71] F. Viana, D. Bayliss, and A. Berger. Multiple potassium conductances and their role in action potential repolarization and repetitive firing behavior of neonatal rat hypoglossal motoneurons. *Journal of Neurophysiology*, 69(6):2150–2163, 1993.

[72] B. P. Vos, R. Maex, A. Volny-Luraghi, and E. De Schutter. Parallel fibers synchronize spontaneous activity in cerebellar golgi cells. *Journal of Neuroscience*, 19:RC6–1, 1999.

[73] R. Winmill and M. Hedrick. Gap junction blockade with carbenoxolone differentially affects fictive breathing in larval and adult bullfrogs. *Respiratory Physiology and Neurobiology*, 138(2-3):239–251, 2003.

[74] U. Wolf, M. Rapoport, and T. Schweizer. Evaluating the affective component of the cerebellar cognitive affective syndrome. *The Journal of Neuropsychiatry and Clinical Neurosciences*, 21(3):245–253, 2009.

[75] J. Zito, H. Memelli, K. G. Horn, I. C. Solomon, and L. D. Wittie. Application of a staggered walk algorithm for generating large-scale morphological neuronal networks. *Computational Intelligence and Neuroscience*, 2012:10, 2012.